

Phonon screening and dissociation of excitons at finite temperatures from first principles

Antonios M. Alvertis,^{1,2} Jonah B. Haber,^{3,2} Zhenglu Li,^{4,2,5} Christopher J. N. Coveney,⁶ Steven G. Louie,^{2,5} Marina R. Filip,⁶ and Jeffrey B. Neaton^{2,5,7,*}

¹KBR, Inc, NASA Ames Research Center, Moffett Field, California 94035, United States

²Materials Sciences Division, Lawrence Berkeley National Laboratory, Berkeley, California 94720, United States

³Department of Materials Science and Engineering,

Stanford University, Stanford, California 94305, United States

⁴Mork Family Department of Chemical Engineering and Materials Science,

University of Southern California, Los Angeles, California 90089, USA

⁵Department of Physics, University of California Berkeley, Berkeley, United States

⁶Department of Physics, University of Oxford, Oxford OX1 3PJ, United Kingdom

⁷Kavli Energy NanoScience Institute at Berkeley, Berkeley, United States

(Dated: August 18, 2024)

The properties of excitons, or correlated electron-hole pairs, are of paramount importance to optoelectronic applications of materials. A central component of exciton physics is the electron-hole interaction, which is commonly treated as screened solely by electrons within a material. However, nuclear motion can screen this Coulomb interaction as well, with several recent studies developing model approaches for approximating the phonon screening to the properties of excitons. While these model approaches tend to improve agreement with experiment for exciton properties, they rely on several approximations that restrict their applicability to a wide range of materials, and thus far they have neglected the effect of finite temperatures. Here, we develop a fully first-principles, parameter-free approach to compute the temperature-dependent effects of phonon screening within the *ab initio* *GW*-Bethe Salpeter equation framework. We recover previously proposed models of phonon screening as well-defined limits of our general framework, and discuss their validity by comparing them against our first-principles results. We develop an efficient computational workflow and apply it to a diverse set of semiconductors, specifically AlN, CdS, GaN, MgO and SrTiO₃. We demonstrate under different physical scenarios how excitons may be screened by multiple polar optical or acoustic phonons, how their binding energies can exhibit strong temperature dependence, and the ultrafast timescales on which they dissociate into free electron-hole pairs.

I. INTRODUCTION

Excitons, correlated electron-hole pairs often generated upon photoexcitation, are critical to semiconductor optoelectronic applications. The dissociation of bound excitons into free charge carriers is central to photovoltaics [1, 2], while their ability to recombine and emit light underpins applications such as light-emitting diodes [3, 4]. Capturing the materials-specific many-body interactions of electrons and holes in solids requires careful theoretical descriptions of screening and scattering mechanisms, and constitutes a major challenge for first-principles approaches. The state-of-the-art *ab initio* framework to describe excitons within many-body perturbation theory is based on the *GW* approximation [5, 6] and Bethe-Salpeter equation (BSE) [7–10] (*GW*+BSE), where *G* is the one-particle Green’s function and *W* is the screened Coulomb interaction. A key ingredient responsible for the formation of bound excitons is the frequency-dependent (ω) screened Coulomb

interaction [9–11]

$$W(\mathbf{r}, \mathbf{r}', \omega) = \int d\mathbf{r}'' \epsilon^{-1}(\mathbf{r}, \mathbf{r}'', \omega) v(\mathbf{r}'', \mathbf{r}'), \quad (1)$$

where *v* is the bare Coulomb interaction and $\epsilon(\mathbf{r}, \mathbf{r}'', \omega)$ is the frequency-dependent, non-local dielectric function. Most commonly, ϵ is obtained within the random-phase approximation (RPA) [12] and describes screening only originating from the perturbation of the electron density in the limit of clamped ions, the *electronic* screening.

However, exciton binding energies computed within the standard *ab initio* *GW*+BSE framework can overestimate experiments, by up to a factor of three in certain heteropolar crystals [13], a discrepancy attributed to the screening of Coulomb interactions due to polar ionic vibrations [13–18], normally neglected in standard approaches. The phonon contribution to the low-frequency (static) dielectric constant, ϵ_0 , in addition to the high-frequency (optical) counterpart, ϵ_∞ , quantifies the screening originating from ionic vibrations. This raises the question of which dielectric constant more appropriately describes the screening of weakly interacting electrons and holes (*i.e.* with a binding energy comparable to phonon energies), with several studies proposing an intermediate *ad hoc* “effective” dielectric constant with a value between these two limits [19–21], in an ef-

* jboneaton@lbl.gov

fort to account for screening from both electrons and phonons and to capture experimental trends. An alternative approach is to modify the dielectric function of Eq. 1 so that it includes the contributions from polar phonons [15, 22]. Several model approaches have been reported that include phonon contributions W^{ph} to the screened Coulomb interaction to complement the standard clamped-ion electronic screening $W = W^{el}$ [19, 23–25]. The results from such approaches can vary significantly depending on approximations that are used; they are limited to the description of screening from polar phonons; and they do not yield detailed microscopic insights into these effects relative to electronic screening. A rigorous, fully first-principles, description of both electronic and phonon screening of excitons on equal footing is therefore necessary to develop truly predictive accuracy for exciton properties in diverse materials, and to reach a deeper understanding of factors affecting the relative importance and interplay of these two effects.

Within many-body perturbation theory and to the lowest order in the electron-phonon interaction, the phonon-screened Coulomb interaction is given by [26–28]

$$W^{ph}(\mathbf{r}, \mathbf{r}', \omega) = \sum_{\mathbf{q}, \nu} D_{\mathbf{q}, \nu}(\omega) g_{\mathbf{q}, \nu}(\mathbf{r}) g_{\mathbf{q}, \nu}^*(\mathbf{r}'), \quad (2)$$

where $D_{\mathbf{q}, \nu}(\omega)$ is the propagator of a phonon with branch index ν at wavevector \mathbf{q} , and $g_{\mathbf{q}, \nu}$ is the electron-phonon vertex. Ref. [25] used this expression to derive a 0 K correction to the electron-hole interaction term in the *ab initio* Bethe-Salpeter equation due to phonon screening, subsequently approximating it for “hydrogenic” excitons and long range polar electron-phonon interactions described by the Fröhlich model. For a number of systems where these approximations are well-justified, this notably improved agreement with experiment for exciton binding energies.

Here, we generalize the framework in Ref. [25] to finite temperatures and implement it within a fully *ab initio* BSE approach, accounting for the effects of phonon screening to lowest order in the electron-phonon interaction, at the level of phonon exchange. Ref. [25] is one of several recent papers [14, 22] that, building on pioneering work of Hedin and Lundqvist [29] and Strinati [11] decades earlier, include the effects of phonon screening on exciton properties, within *ab initio* many-body perturbation theory. Closely related recent works treat exciton-phonon interactions in a modern first-principles context, and using cumulants [30], using two-particle Green’s functions [31] and using a linear-response real-time framework [32], have derived phonon-renormalized exciton properties in terms of the exciton-phonon vertex, analogous to the one used in the seminal work of Toyozawa [33]. Some recent *ab initio* calculations of exciton-phonon interactions in solids capture phenomena such as phonon-assisted absorption and luminescence [34–36], temperature-dependent exciton localization [37] and shifts of the exciton energy [38], and report

exciton-exciton scattering rates [39–41]. Here, starting from Eq. 2, we develop and implement a temperature-dependent complex correction to the standard clamped-ion BSE kernel, referred to in what follows as the *phonon kernel*, K_{ph} . Although it is possible to recover or go beyond the exciton-phonon self-energy of Ref. [31] starting from W_{ph} by including other higher-order diagrams in the BSE [30], here we retain only the phonon exchange diagram of Ref. [31] (equivalently Eq. 2), a judicious, computationally efficient, and physical low-order approximation for semiconductor systems (Ref. [24]) for which free electron- and hole-polaron radii (as described by Fan-Migdal diagrams) are on the same order as exciton radii [19, 42]. As we show in what follows, within the limits of perturbation theory, the real part of K_{ph} in the exciton basis provides a quantitative prediction of the temperature-dependent renormalization of exciton (binding) energies via phonon screening, and the imaginary part can lead to a quantitative rate of dissociation of an exciton into free electron and holes through absorption of a phonon within the approximations made here.

Demonstrating this in a select set of semiconductors, we predict that phonons are responsible for a 50% reduction of the exciton binding energy of CdS at room temperature, an effect that is highly temperature-dependent, with acoustic phonons having a substantial contribution. Moreover, we predict that phonon absorption by excitons in GaN contribute to their ultrafast dissociation into free charge carriers with a timescale that is consistent with experimental measurements for similar materials. In SrTiO₃, we find multiple polar phonons can contribute to the screening of excitons at once, leading to a significant overall reduction of the exciton binding energy. Finally, we show how approximations to our first-principles results lead to models that are commonly used in the literature, such as the Haken potential [23, 24], and we discuss the validity of these models for different systems.

The structure of this paper is as follows. Section II presents the theoretical background of our work and summarizes the derivation of the first-principles phonon correction to the BSE kernel at finite temperatures, while Sections II A and II B focus on the real and imaginary parts of this kernel respectively, and the observables that may be extracted from these quantities. Appendix A summarizes exciton and polaron radii of the systems studied as a part of this work, as estimated within the Wannier-Mott and weakly coupled Fröhlich polaron regime respectively, which justifies certain approximations appearing in Section II A. Appendix B provides a more in-depth look into the imaginary part of the phonon kernel and its physical interpretation. In Section III we examine different approximations to the phonon kernel, and connect our work to model results from the literature. In Section IV we present the bulk of our computational results. Specifically, Section IV A provides relevant computational details, while Section IV B presents our first-principles results at 0 K for a range of systems, and

compares these to the predictions of various models of phonon screening, also discussing the origin of observed differences. Section IV C presents an in-depth application of our *ab initio* workflow to selected materials and their temperature-dependent phonon screening and exciton dissociation properties. For these selected systems, the convergence of their phonon screening properties is demonstrated in detail in Appendix C. For SrTiO₃ we compare the *ab initio* and model results in greater detail in Appendix E. Additionally, Section IV D quantifies the importance of acoustic phonons in screening excitons and the importance of piezoelectric interactions. Finally in Section V, we provide a discussion and outlook for our work.

II. FIRST-PRINCIPLES PHONON KERNEL

The Bethe-Salpeter equation (BSE) within the Tamm-Dancoff approximation for zero-momentum excitons in reciprocal space is written as [10]

$$(E_{c\mathbf{k}} - E_{v\mathbf{k}})A_{c\mathbf{v}\mathbf{k}}^S + \sum_{c'\mathbf{v}'\mathbf{k}'} \langle c\mathbf{v}\mathbf{k} | K^{eh} | c'\mathbf{v}'\mathbf{k}' \rangle A_{c'\mathbf{v}'\mathbf{k}'}^S \quad (3)$$

$$= \Omega^S A_{c\mathbf{v}\mathbf{k}}^S,$$

where $E_{c\mathbf{k}}$ and $E_{v\mathbf{k}}$ are the quasiparticle energies of conduction and valence bands, respectively. The BSE of Eq. 3 describes excited states accounting only for electronic screening effects, and will hence be referred to as the “bare” BSE, to distinguish it from the case where phonon screening is included. The coefficients $A_{c\mathbf{v}\mathbf{k}}^S$ describe the corresponding excited state S with excitation energy Ω_S as a linear combination of free electron-hole pair wave functions ($|c\mathbf{v}\mathbf{k}\rangle$, typically obtained from a density functional theory (DFT) calculation), namely

$$|S\rangle = \sum_{c\mathbf{v}\mathbf{k}} A_{c\mathbf{v}\mathbf{k}}^S |c\mathbf{v}\mathbf{k}\rangle. \quad (4)$$

The kernel K^{eh} describes the interaction between electrons and holes and consists of direct (d) and exchange (x) contributions, $K^{eh} = K^d + K^x$. The repulsive exchange term K^x depends on the bare Coulomb interactions and is frequency-independent. In the absence of spin-orbit coupling, this term is only non-zero for excitons of zero spin, and is responsible for the different properties of singlet and triplet excitons [10]. On the other hand, the direct term is attractive, frequency-dependent, and involves the screened Coulomb interaction W . This term can be written as

$$K_{c\mathbf{v}\mathbf{k},c'\mathbf{v}'\mathbf{k}'}^d(\Omega) = -\langle c\mathbf{v}\mathbf{k} | \frac{i}{2\pi} \int d\omega e^{-i\omega\delta} W(\mathbf{r}, \mathbf{r}', \omega) \times \quad (5)$$

$$\left[\frac{1}{\Omega - \omega - \Delta_{c'\mathbf{k}'v\mathbf{k}} + i\delta} + \frac{1}{\Omega + \omega - \Delta_{c\mathbf{v}v'\mathbf{k}'} + i\delta} \right] |c'\mathbf{v}'\mathbf{k}'\rangle,$$

where δ is a small real and positive number and we have introduced the notation $\Delta_{c\mathbf{k}v\mathbf{k}} = E_{c\mathbf{k}} - E_{v\mathbf{k}}$. This kernel term is usually computed in the clamped-ion limit including only electronic screening, *i.e.* $W = W^{el}$ [9, 10]. While W^{el} is fully frequency-dependent in principle, since exciton binding energies are much smaller than the band gaps and the plasmon energies in many insulators, the dynamical properties of W^{el} are often neglected for weakly-bound excitons [10], namely $K_{c\mathbf{v}\mathbf{k},c'\mathbf{v}'\mathbf{k}'}^{el}(\Omega_S) = \langle c\mathbf{v}\mathbf{k} | W^{el}(\mathbf{r}, \mathbf{r}', \omega = 0) | c'\mathbf{v}'\mathbf{k}' \rangle$. Dynamical effects can be important in some cases, for example in order to account for free carrier screening from acoustic plasmons [43–45].

We now include the contribution of phonon screening to the kernel, taking $W = W^{el} + W^{ph}$, which will yield a correction K^{ph} to the direct kernel of Eq. 5. To obtain this phonon kernel K^{ph} , we introduce the phonon screening of Eq. 2 into Eq. 5, with the phonon propagator appearing in Eq. 2 written as [46]

$$D_{\mathbf{q},\nu}(\omega) = \frac{1}{\omega - \omega_{\mathbf{q},\nu} + i\delta} - \frac{1}{\omega + \omega_{\mathbf{q},\nu} - i\delta}. \quad (6)$$

Therefore, as in Ref. [25], we arrive to the following expression for the phonon kernel

$$K_{c\mathbf{v}\mathbf{k},c'\mathbf{v}'\mathbf{k}'}^{ph}(\Omega) = - \sum_{\mathbf{q},\nu} g_{cc'\nu}(\mathbf{k}', \mathbf{q}) g_{vv'\nu}^*(\mathbf{k}', \mathbf{q}) \times \quad (7)$$

$$\left[\frac{1}{\Omega - \Delta_{c\mathbf{v}\mathbf{k}'\mathbf{k}'} - \omega_{\mathbf{q},\nu} + i\eta} + \frac{1}{\Omega - \Delta_{c'\mathbf{k}'v\mathbf{k}} - \omega_{\mathbf{q},\nu} + i\eta} \right],$$

where η a small real and positive number. Here $\mathbf{q} = \mathbf{k} - \mathbf{k}'$ and $g_{nm\nu}(\mathbf{k}', \mathbf{q}) = \langle n\mathbf{k}' + \mathbf{q} | g_{\mathbf{q}\nu} | m\mathbf{k}' \rangle$, which can be computed, for example, via density functional perturbation theory (DFPT) [47] or beyond, via *GW* perturbation theory (GWPT) [48].

The result of Eq. 7 is only valid at zero temperature. We extend the phonon kernel to finite temperatures via the Matsubara formalism. Here the integral of Eq. 5 is analytically continued into the complex plane and evaluated at imaginary bosonic Matsubara frequencies. Following this well-established procedure [46], we obtain the following expression for the temperature-dependent

phonon contribution to the kernel

$$K_{cv\mathbf{k},c'v'\mathbf{k}'}^{ph}(\Omega, T) = - \sum_{\mathbf{q}, \nu} g_{cc'\nu}(\mathbf{k}', \mathbf{q}) g_{vv'\nu}^*(\mathbf{k}', \mathbf{q}) \times \quad (8)$$

$$\left[\frac{N_B(\omega_{\mathbf{q}, \nu}, T) + 1 + N_B(\Delta_{c\mathbf{k}v'\mathbf{k}', T})}{\Omega - \Delta_{c\mathbf{k}v'\mathbf{k}' - \omega_{\mathbf{q}, \nu} + i\eta} + \frac{N_B(\omega_{\mathbf{q}, \nu}, T) + 1 + N_B(\Delta_{c'\mathbf{k}'v\mathbf{k}, T})}{\Omega - \Delta_{c'\mathbf{k}'v\mathbf{k} - \omega_{\mathbf{q}, \nu} + i\eta} + \frac{N_B(\omega_{\mathbf{q}, \nu}, T) - N_B(\Delta_{c\mathbf{k}v'\mathbf{k}', T})}{\Omega - \Delta_{c\mathbf{k}v'\mathbf{k}' + \omega_{\mathbf{q}, \nu} + i\eta} + \frac{N_B(\omega_{\mathbf{q}, \nu}, T) - N_B(\Delta_{c'\mathbf{k}'v\mathbf{k}, T})}{\Omega - \Delta_{c'\mathbf{k}'v\mathbf{k} + \omega_{\mathbf{q}, \nu} + i\eta} \right],$$

where N_B is the Bose-Einstein occupation factor at temperature T . As we are concerned with temperatures near room temperature and materials with band gaps that are large compared to phonon energies, we use the fact that $N_B(\Delta_{c\mathbf{k}v\mathbf{k}}, T) \ll N_B(\omega_{\mathbf{q}, \nu}, T)$ moving forward.

The first two terms within the bracket of Eq. 8 describe the contribution of phonon emission to the kernel, and these terms are finite even at 0 K. The last two terms within the bracket of Eq. 8 are due to the absorption of phonons, and are only non-zero at temperatures greater than zero. In this work, we implement the *ab initio* phonon kernel (as a matrix) rewritten in the bare or unperturbed exciton basis as

$$K_{S,S'}^{ph}(\Omega, T) = - \sum_{cv\mathbf{k},c'v'\mathbf{k}'} A_{cv\mathbf{k}}^{S*} g_{cc'\nu}(\mathbf{k}', \mathbf{q}) g_{vv'\nu}^*(\mathbf{k}', \mathbf{q}) A_{c'v'\mathbf{k}'}^{S'} \times \quad (9)$$

$$\left[\frac{N_B(\omega_{\mathbf{q}, \nu}, T) + 1}{\Omega - \Delta_{c\mathbf{k}v'\mathbf{k}' - \omega_{\mathbf{q}, \nu} + i\eta} + \frac{N_B(\omega_{\mathbf{q}, \nu}, T) + 1}{\Omega - \Delta_{c'\mathbf{k}'v\mathbf{k} - \omega_{\mathbf{q}, \nu} + i\eta} + \frac{N_B(\omega_{\mathbf{q}, \nu}, T)}{\Omega - \Delta_{c\mathbf{k}v'\mathbf{k}' + \omega_{\mathbf{q}, \nu} + i\eta} + \frac{N_B(\omega_{\mathbf{q}, \nu}, T)}{\Omega - \Delta_{c'\mathbf{k}'v\mathbf{k} + \omega_{\mathbf{q}, \nu} + i\eta} \right],$$

where the off-diagonal matrix elements of $K_{S,S'}^{ph}$ describe the extent to which the exciton-phonon scattering significantly changes the character of the excited state S . In the cases we study, off-diagonal contributions to the K^{ph} matrix are negligible, and we therefore do not include them in the following discussions. It should also be noted that since here we work within many-body perturbation theory, this scheme might lead to a poorer descriptions of system with strong non-perturbative electron-phonon coupling. Moreover, multi-phonon processes, which are not captured here, can become significant near room temperature for certain systems [49].

As elaborated on in Section IV A, converging the phonon screening properties requires the sum of Eq. 9 to be computed on a dense grid in reciprocal space. Wannier-Fourier interpolation can be utilized to greatly accelerate the calculation of electron-phonon matrix elements g via DFPT on a dense grid [50]. However, as Wannier interpolation introduces a gauge inconsistency

between the values of g and the exciton coefficients, it has not so far been possible to take advantage of Wannier-based techniques to compute exciton-phonon interactions from first-principles [39, 40, 51, 52]. To address this challenge [53], we use the strategy of computing the exact same set of Wannier-interpolated wavefunctions from DFT on a fine k-grid, and use their plane-wave basis representation to perform BSE calculations with the BerkeleyGW code [54], and their Wannier basis representation to obtain electron-phonon matrix elements on the same fine k-grid from DFPT using the EPW code [55]. Consequently, the gauge consistency is naturally guaranteed. Our work combines for the first time Wannier interpolation methods for electron-phonon and electron-hole interactions from first principles. Not only does our approach greatly accelerate our calculations, but it gives us access to the study of systems such as SrTiO₃ and the nitrides GaN and AlN, which would otherwise be computationally prohibitive.

Overall, inclusion of phonon screening in Eq. 3 leads to the following generalized BSE

$$(E_{c\mathbf{k}} - E_{v\mathbf{k}}) A_{cv\mathbf{k}}^{S,ph} \quad (10)$$

$$+ \sum_{c'v'\mathbf{k}'} \langle cv\mathbf{k} | K^{eh} + K^{ph}(\omega, T) | c'v'\mathbf{k}' \rangle A_{c'v'\mathbf{k}'}^{S,ph}$$

$$= \Omega^{S,ph} A_{cv\mathbf{k}}^{S,ph}.$$

The superscript in the eigenvalues and eigenvectors $\Omega^{S,ph}, A^{S,ph}$ highlights that the excited states S arising from the solution of Eq. 10 now include the effect of phonon screening. While one can diagonalize the combined kernel $K = K^{eh} + K^{ph}$ to find the solutions of Eq. 10, for the systems considered in this work it is an excellent approximation to consider the effect of phonon screening as a small perturbation. We will therefore obtain the effect of phonon screening on excited states within first-order perturbation theory in this work, as discussed in the following Section II A.

A. Real part of the phonon kernel

For non-degenerate excitons of energy Ω_S , the correction to their energies from phonon screening within first-order perturbation theory is

$$\Delta\Omega_S = \text{Re} \left[\langle S | K^{ph}(\Omega_S) | S \rangle \right]. \quad (11)$$

For a subspace of degenerate excitons with dimension N_S , the phonon screening correction to the exciton energies is taken to be equal to the normalized trace of the $N_S \times N_S$ K^{ph} matrix, calculated as $\Delta\Omega_S = \frac{1}{N_S} \text{Tr}[K^{ph}(\Omega_S)]$, which is gauge-invariant. Higher-order corrections to the exciton energy due to phonon screening at the level of Eq. 2 are unimportant, since these are proportional to the off-diagonal matrix elements of $K_{S,S'}^{ph}$, which for all

systems studied here are of the order of $10^{-3} - 10^{-2}$ meV and can be safely neglected. For the same reason, first-order corrections to exciton wavefunctions are negligible, and we therefore focus in what follows on computing the correction of Eq. 11 to the exciton energies.

We note here that in principle the effect of phonon screening should also be included in the GW self-energy, yielding a correction iGW^{ph} to the quasiparticle band structure, and $E_{c\mathbf{k}}, E_{v\mathbf{k}}$ in Eq. 10. This frequency- and temperature-dependent correction is equivalent to the one described by the so-called Fan-Migdal self-energy [30], Σ^{FM} , the real part of which captures low-order energy renormalization and mass enhancement due to electron-phonon interactions [50]. Therefore, if one were to include the effect of phonon screening both in the GW self-energy and in the BSE kernel this would generalize the BSE of Eq. 10 so that the bare electron and hole energies are substituted by the respective polaron energies $\tilde{E}_{c\mathbf{k}} = E_{c\mathbf{k}} + \Sigma_c^{FM}(\omega, T)$ and $\tilde{E}_{v\mathbf{k}} = E_{v\mathbf{k}} + \Sigma_v^{FM}(\omega, T)$. Ref. [56] included such a temperature dependence for the quasiparticle energies, however did not account for the contribution of phonon screening to excitons.

The exciton-phonon interaction was described in Ref. [31] as the sum of three distinct contributions to the self-energy: the dynamical Fan-Migdal term, the dynamical phonon exchange term, and the frequency-independent Debye-Waller term. We note that the phonon exchange term in Ref. [31] is equivalent to Eq. 8 and that the Debye-Waller term does not affect the exciton binding energy. Thus, inclusion of the phonon kernel and the Fan-Migdal term in the BSE would be consistent with Ref. [31]. Our approach is distinct from that of Ref. [32], which presented an alternative derivation of the exciton-phonon self-energy, based on a BSE in which an optical response function is defined as the variation of the electronic density with respect to the total potential (rather than only the external potential, as in Ref. [31]); the use of this alternative approach was reported to lead to small differences in computed exciton linewidths for monolayer MoS₂ and MoSe₂ [32]. While a deeper comparison of the distinct approaches of Ref. [31] and Ref. [32] is reserved for future work, we expect that, quantitatively, changes to the exciton-phonon interaction originating from different formulations of the BSE will be small compared with the effects of phonon screening, given our *ab initio* results in Section IV and the results in Ref. [32]. Moreover, we note that the exciton-phonon self-energy of Ref. [32] also contains a phonon exchange diagram that is equivalent to that of Ref. [31] and central to our work here.

Neglecting the Fan-Migdal term of the exciton-phonon self-energy ([31, 32]) in constructing K_{ph} is acceptable here because, by itself, this term, which describes the induced lattice polarization around the exciton's constituent electron and hole as if the two particles were independent, fails to capture any modifications of the lattice polarization when the electron and hole are bound to-

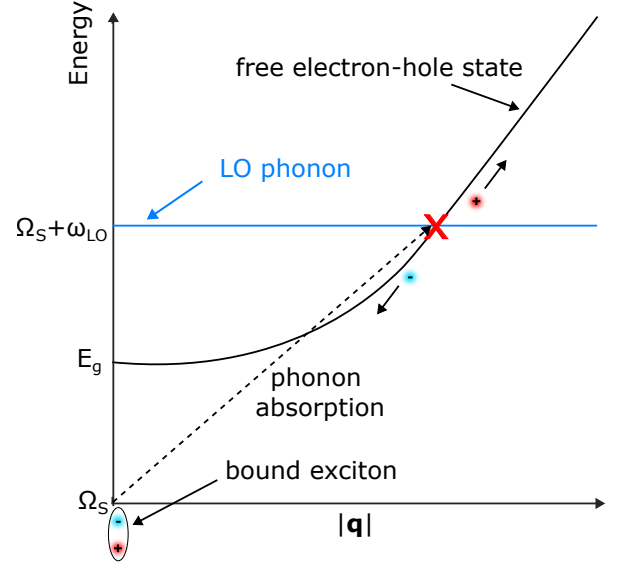


FIG. 1. Schematic of the exciton dissociation process described by Eq. 16 when a material with a band gap of E_g and exciton energy Ω_S absorbs a longitudinal optical (LO) phonon of frequency ω_{LO} , and the condition $\Omega_S + \omega_{LO} > E_g$ is satisfied.

gether. As noted originally in Ref. [19, 42] and reiterated recently in Ref. [25], depending on the relative exciton and electron (hole) polaron radii, the lattice polarization associated with the polarons may interfere significantly, and even possibly cancel each other. For several semiconductors, including those studied in this work, exciton and electron (hole) polaron radii have similar estimated values (see Appendix A), strongly suggesting that naive inclusion of the Fan-Migdal term at lowest order while ignoring interference effects that enter at higher order will lead to significant errors. We therefore restrict our focus to phonon exchange, and reserve a more rigorous treatment of polaronic mass enhancement and interference effects ([19, 42]) for future work. Thus, in what follows, the phonon screening shift of the lowest bound exciton energy, $\Delta\Omega_S$, as obtained through Eq. 11, is given by the reduction of the exciton binding energy of the same magnitude, *i.e.* $\Delta E_B = -\Delta\Omega_S$.

B. Imaginary part of the phonon kernel

The phonon kernel of Eq. 9 is a complex quantity. For phonon emission and for $\omega = \Omega_S$, the imaginary part of the phonon kernel is proportional to

$$\delta[\Omega_S - \omega_{\mathbf{q},\nu} - (E_{c\mathbf{k}'} - E_{v\mathbf{k}})] + \delta[\Omega_S - \omega_{\mathbf{q},\nu} - (E_{c\mathbf{k}} - E_{v\mathbf{k}'})], \quad (12)$$

while for absorption it is proportional to

$$\delta[\Omega_S + \omega_{\mathbf{q},\nu} - (E_{c\mathbf{k}'} - E_{v\mathbf{k}})] + \delta[\Omega_S + \omega_{\mathbf{q},\nu} - (E_{c\mathbf{k}} - E_{v\mathbf{k}'})]. \quad (13)$$

For excitons of zero momentum, the conservation of

energy condition, $\Omega_S - \omega_{\mathbf{q},\nu} = E_{c\mathbf{k}'} - E_{v\mathbf{k}}$, which must be met for the emission channel to make non-zero contributions to the imaginary part of the phonon kernel, may only be satisfied for so-called “resonant” excitons with energies greater than the quasiparticle band gap. This could occur for indirect band gap materials with resonant excitons above the fundamental gap, *e.g.* silver-pnictogen halide double perovskites [57]. Alternatively, this condition may be satisfied for higher-lying exciton states in the continuum, the analysis of which is beyond the scope of the present study. On the other hand, phonon absorption, $\Omega_S + \omega_{\mathbf{q},\nu} = E_{c\mathbf{k}'} - E_{v\mathbf{k}}$, can occur if the energy of an exciton which has absorbed a phonon matches that of a free electron-hole pair, as schematically depicted in Fig. 1 for the example of a longitudinal optical (LO) phonon with frequency ω_{LO} . Specifically, this condition is only satisfied in a single-phonon process if the absorbed phonon has a greater or equal frequency than the exciton binding energy, *i.e.* $\omega_{\mathbf{q},\nu} \geq E_B$.

The imaginary part of the exciton-phonon self-energy contains information about the lifetime of excitons due to scattering from phonons into other excitons or free electron-hole pairs [31]. As motivated in Fig. 1, the phonon kernel describes scattering from an initial exciton state to a final free electron-hole pair, primarily due to phonon absorption. This process can be formally described within many-body perturbation theory and scattering theory by an \mathcal{S} -matrix of the following form [46, 58]

$$\mathcal{S} = 2\pi i \delta[\Omega_S + \omega_{\mathbf{q},\nu} - (E_{c\mathbf{k}} - E_{v\mathbf{k}'})] \times \langle (c\mathbf{k}, v\mathbf{k}'), N_B | K^{ph} | S, N_B + 1 \rangle. \quad (14)$$

The rate τ_S^{-1} of this scattering process described by the \mathcal{S} -matrix of Eq. 14 is obtained by taking the time derivative of the square magnitude of this expression. Using the fact that $\delta^2[\Omega_S + \omega_{\mathbf{q},\nu} - (E_{c\mathbf{k}} - E_{v\mathbf{k}'})] = \lim_{t \rightarrow \infty} \frac{t}{2\pi} \delta[\Omega_S + \omega_{\mathbf{q},\nu} - (E_{c\mathbf{k}} - E_{v\mathbf{k}'})]$, we arrive at

$$\tau_S^{-1} \approx 2\pi \sum_{c\mathbf{k}v\mathbf{k}'} \delta[\Omega_S + \omega_{\mathbf{q},\nu} - (E_{c\mathbf{k}} - E_{v\mathbf{k}'})] \times |\langle (c\mathbf{k}, v\mathbf{k}'), N_B | K^{ph} | S, N_B + 1 \rangle|^2, \quad (15)$$

in atomic units, where the approximately equal symbol is used because of making the Born approximation, as detailed in Appendix B. Eq. 15 is the same expression as that obtained through the application of Fermi’s golden rule for exciton dissociation, from an initial bound exciton ($|S, N_B + 1\rangle$) to a final free electron-hole ($|(c\mathbf{k}, v\mathbf{k}'), N_B\rangle$) state. This is analogous to the elementary treatment of the photoelectric effect in the hydrogen atom [59].

Defining this scattering process through the \mathcal{S} -matrix of Eq. 14 generally requires the initial and final states to be orthogonal to each other [60]. We can ensure this is the case within the Born approximation using the theory of rearrangement collisions [61–63], as discussed in more detail in Appendix B and to be presented in Ref. [64].

Employing the optical theorem for the \mathcal{S} -matrix of Eq. 14, the quantity $\text{Im}[K_{SS}^{ph}(\Omega_S, T)]$ can be shown to be equivalent to the rate of the exciton dissociation process depicted in Fig. 1, *i.e.*

$$2|\text{Im}[K_{SS}^{ph}(\Omega_S, T)]| \approx \tau_S^{-1}(T). \quad (16)$$

Thus, our framework enables the *ab initio* calculation of exciton dissociation timescales for this particular channel for cases in which phonons with $\omega_{\mathbf{q},\nu} > E_B$ dominate. In this regime $\omega_{\mathbf{q},\nu} > E_B$ exciton dissociation competes with phonon-mediated exciton-exciton scattering, while exciton-exciton scattering dominates when $\omega_{\mathbf{q},\nu} < E_B$. In what follows below, we will discuss GaN, a system with ultra-fast exciton dissociation.

III. APPROXIMATIONS TO THE REAL PART OF THE PHONON KERNEL

Having established our first-principles formalism to compute the phonon kernel, we now explore several common approximations to the real part of this quantity, *i.e.* the perturbative correction ΔE_B to the exciton binding energy due to phonon screening, at $T = 0$ K. The discussion of these approximations to ΔE_B reveals key physical intuition and connects our work to previous studies. Since for this analysis we restrict ourselves to zero temperatures, we only describe the effect of phonon emission on exciton binding energies.

A. Fröhlich electron-phonon coupling and hydrogenic excitons

Several semiconductors of interest for optoelectronics, such as halide perovskites [25], exhibit electron-phonon coupling dominated by long-range interactions with polar ionic vibrations, which can be described within the Fröhlich model by the operator [65]

$$g_{\mathbf{q}}^F(\mathbf{r}) = \frac{i}{|\mathbf{q}|} \left[\frac{4\pi}{NV} \frac{\omega_{LO}}{2} \left(\frac{1}{\epsilon_\infty} - \frac{1}{\epsilon_0} \right) \right]^{\frac{1}{2}} e^{i\mathbf{q}\cdot\mathbf{r}}, \quad (17)$$

where N is the number of unit cells and V the unit cell volume.

Additionally, excitons of a wide class of materials behave in a hydrogenic manner according to the Wannier-Mott limit [66, 67], with the reciprocal space wavefunction of their first excited state ($1s$) expressed as

$$A_{\mathbf{k}} = \frac{(2a_o)^{3/2}}{\pi} \cdot \frac{1}{(1 + a_o^2 k^2)^2}, \quad (18)$$

where $a_o = 1/(2E_B\mu)^{1/2}$ the exciton Bohr radius (in atomic units), \mathbf{k} the wavevector, and μ the exciton effective mass $1/\mu = 1/m_e + 1/m_h$, with m_e and m_h the effective

tive mass of the electron and hole, respectively. Defining the exciton binding energy as $E_B = E_g - \Omega_S$, where E_g is the direct fundamental gap, assuming dispersive parabolic bands for the conduction and valence states, and ignoring the dispersion of the LO phonon, we arrive at the expression [25]:

$$\Delta E_B = -\frac{8a_o^3}{\pi^2} \sum_{\mathbf{k}\mathbf{q}} \frac{|g_{\mathbf{q}\nu}|^2}{[1 + a_o^2 k^2]^2 [1 + a_o^2 |\mathbf{k} + \mathbf{q}|^2]^2} \times \left[\frac{1}{E_B + \frac{k^2}{2m_e} + \frac{|\mathbf{k} + \mathbf{q}|^2}{2m_h} + \omega_{LO}} + \frac{1}{E_B + \frac{|\mathbf{k} + \mathbf{q}|^2}{2m_e} + \frac{k^2}{2m_h} + \omega_{LO}} \right]. \quad (19)$$

In what follows, we compute this expression numerically for several systems on a grid of \mathbf{k} -/ \mathbf{q} -points and we term the corresponding correction as $\Delta E_B^{\text{F-H}}$ (due to using the Fröhlich and hydrogenic approximations), in order to differentiate it from the full *ab initio* calculation.

A way to further simplify Eq. 19, and derive analytic expressions for ΔE_B , is to take the limits $\mathbf{k}/\mathbf{q} \rightarrow \mathbf{0}$. In Sections III B and III C, we explore these limits.

B. The $\mathbf{k} \rightarrow 0$ limit and the Haken potential

Following Strinati [11], for excitons that are peaked around $\mathbf{k} = \mathbf{0}$, we can consider the $\mathbf{k} \rightarrow \mathbf{0}$ limit of Eq. 19 and obtain

$$\Delta E_B = \langle 1s | V_{GH}(r) | 1s \rangle, \quad (20)$$

where $|1s\rangle$ is the hydrogenic wavefunction and the potential V_{GH} is given by

$$V_{GH}(r) = v(r) \frac{\omega_{LO}}{2\epsilon_*(\omega_{LO} + E_B)} (e^{-r/\tilde{r}_e} + e^{-r/\tilde{r}_h}), \quad (21)$$

with $v(r)$ the bare Coulomb potential and $\frac{1}{\epsilon_*} = (\frac{1}{\epsilon_\infty} - \frac{1}{\epsilon_0})$. The subscript of the potential term V_{GH} indicates this is a generalized Haken potential, having the same form of the so-called Haken potential [23, 24], with the exception that V_{GH} retains the exciton binding energy, which is considered negligible in the derivation presented in Ref. [11]. We have defined the modified polaron radii for the electron and hole, compared to the usual definition [20], as $\tilde{r}_{e,h} = \frac{1}{\sqrt{2m_{e,h}(\omega_{LO} + E_B)}}$, retaining the exciton binding energy. Therefore, the Haken potential is trivially recovered as an approximation of our *ab initio* phonon screening expression, via a simplification of Eq. 19.

With the additional approximation $m_e = m_h$, the expectation value for the shift of the exciton energy due to

phonon screening can be expressed in this limit as

$$\Delta E_B^{\mathbf{k} \rightarrow \mathbf{0}} = -\frac{2\omega_{LO} \left(1 - \frac{\epsilon_\infty}{\epsilon_0}\right)}{\left(1 + \frac{\omega_{LO}}{E_B}\right) \left(1 + \frac{1}{\sqrt{2}} \sqrt{1 + \frac{\omega_{LO}}{E_B}}\right)^2}. \quad (22)$$

C. The $\mathbf{q} \rightarrow 0$ limit

While the Haken potential is based on taking $\mathbf{k} \rightarrow \mathbf{0}$ with the justification of a highly localized exciton in reciprocal space, Ref. [25] instead retained the \mathbf{k} dependence and considered the limit $\mathbf{q} \rightarrow \mathbf{0}$ for the potential term in the expectation value of Eq. 19 for the shift of the exciton binding energy. This is more justified in materials with highly dispersive electronic bands, where setting the electronic momentum to zero can constitute an oversimplification. For such systems, the momentum \mathbf{q} of a phonon may be considered negligible compared to that of an electron or a hole. Using this approximation we obtain

$$\Delta E_B = \langle 1s | V^{\mathbf{q} \rightarrow \mathbf{0}}(r) | 1s \rangle, \quad (23)$$

where

$$V^{\mathbf{q} \rightarrow \mathbf{0}}(r) = v(r) \frac{a_o^2 \omega_{LO}}{\epsilon_*(\omega_{LO} + E_B)} \cdot \left[\frac{1}{a_o^2 - b_o^2} - \frac{1}{r} \cdot \frac{2a_o b_o^2}{(a_o^2 - b_o^2)^2} (1 - e^{-(\frac{1}{b_o} - \frac{1}{a_o})r}) \right], \quad (24)$$

with a_o the exciton Bohr radius and $b_o = \sqrt{\frac{1}{2\mu(\omega_{LO} + E_B)}}$. By setting $m_e = m_h$, the expectation value of Eq. 23 is found to be

$$\Delta E_B^{\mathbf{q} \rightarrow \mathbf{0}} = -2\omega_{LO} \left(1 - \frac{\epsilon_\infty}{\epsilon_0}\right) \frac{\sqrt{1 + \frac{\omega_{LO}}{E_B}} + 3}{\left(1 + \sqrt{1 + \frac{\omega_{LO}}{E_B}}\right)^3}, \quad (25)$$

the result derived in Ref. [25]. We will see in Section IV that this limit yields results which are generally significantly closer to the full *ab initio* value for the shift of the exciton energy compared to the generalized Haken ($\mathbf{k} \rightarrow \mathbf{0}$) case.

IV. AB INITIO RESULTS FOR SELECT SYSTEMS

A. Computational Details

Table I summarizes the different systems studied in this work, the specific structure in which these are studied,

Material	Structure	a (Å)	c/a	Space Group	Identifier
AlN	Wurtzite	3.128	1.604	P6 ₃ mc	mp-661
CdS	Zincblende	4.200	1	F43m	mp-2469
GaN	Wurtzite	3.215	1.630	P6 ₃ mc	mp-804
MgO	Halite, Rock Salt	3.010	1	Fm3m	mp-1265
SrTiO ₃	Cubic Perovskite	3.852	1	Pm3m	mp-5229

TABLE I. Studied materials, their structure, lattice parameters, space group, and identifier in the Materials Project database [68]. We performed geometry optimization for the atomic positions of these systems using DFT within the PBE exchange-correlation functional, keeping their lattice parameters fixed, with the exception of SrTiO₃, for which we used the local density approximation (LDA) and optimized both the atomic positions and its lattice parameter (the LDA has been discussed in the literature to yield more accurate results for structural properties of SrTiO₃ compared to PBE [69]).

their lattice parameter, as well as their space group and identifier in the Materials Project database [68]. For all studied materials with the exception of SrTiO₃, we start by performing a geometry optimization of their atomic positions, leaving the lattice parameters fixed. For this we employ DFT, as implemented within the Quantum Espresso software package [70], and we use the generalized gradient approximation (GGA) as formulated by Perdew, Burke and Ernzerhof (PBE) [71]. For SrTiO₃ we employ the local density approximation (LDA) [72] and optimize both the atomic positions and lattice parameters of this system; the LDA has been discussed in the literature to yield more accurate results for the phonon properties of SrTiO₃ compared to PBE [69]. We then employ DFPT using PBE, with the exception of SrTiO₃ for which we employ LDA to compute the phonon dispersions of the studied materials on a $6 \times 6 \times 6$ grid of \mathbf{q} -points. Using the DFT-PBE Kohn-Sham wavefunctions (LDA for SrTiO₃) as a starting point, we perform GW calculations as implemented within the BerkeleyGW code [54], choosing the calculation parameters to converge the quasiparticle band gaps within 0.1 eV, following Refs. [25, 73] and using a generalized plasmon pole model [6] to compute the dielectric function at finite frequencies. Specifically, we employ the following parameters for the GW calculation: AlN (400 bands, 32 Ry polarizability cutoff, $6 \times 6 \times 6$ half-shifted k-grid), CdS (500 bands, 40 Ry polarizability cutoff, $6 \times 6 \times 6$ half-shifted k-grid), GaN (400 bands, 40 Ry polarizability cutoff, $4 \times 4 \times 4$ half-shifted k-grid), MgO (600 bands, 50 Ry polarizability cutoff, $6 \times 6 \times 6$ Γ -centered k-grid), SrTiO₃ (1000 bands, 14 Ry polarizability cutoff, $6 \times 6 \times 6$ half-shifted k-grid).

The electronic BSE kernel is computed on the same \mathbf{k} -grid as the GW eigenvalues, for three valence and a single conduction band, with the exception of SrTiO₃, where nine valence bands and three conduction bands are employed instead. For all cases, we use the patched sampling technique [74] to interpolate the kernel onto a patch drawn from a fine $100 \times 100 \times 100$ grid, converging the size of the patch to ensure an accuracy of 1 meV or better for the exciton binding energy, as described in detail in Ref. [74]. We find that a patch around Γ with a crystal coordinate cutoff of 0.09 is sufficient to converge the observables of interest in this study for all systems

but MgO and SrTiO₃. For these two systems we extrapolate to the $N_k \rightarrow \infty$ limit by following the convergence rate of the value of $\Delta E_B^{\text{F-H}}$ obtained through the numerical integration of Eq. 19 (see Appendix C). Moreover, we employ Wannier-Fourier interpolation [50] in order to obtain the electron-phonon matrix elements $g_{mn\nu}(\mathbf{k}, \mathbf{q})$ on the same fine patch for the \mathbf{k} - and \mathbf{q} -grid, using modified versions of the Wannier90 [75] and EPW [55] codes, in order to ensure the gauge consistency of the electron-phonon matrix elements computed from EPW and the exciton coefficients computed using BerkeleyGW, using a workflow that will be described elsewhere [53].

B. Comparison between *ab initio* and limiting cases at 0 K.

We start with the *ab initio* phonon screening correction to the exciton binding energy at 0 K, and the values predicted through the various approximations outlined in Section III. The results are summarized in Table II.

Firstly, we note that for all studied systems, the *ab initio* value for the shift of the exciton binding energy due to phonon screening (as given by eq. 11) falls between the values of the two limiting cases $\Delta E_B^{k \rightarrow 0}$ and $\Delta E_B^{q \rightarrow 0}$. The former of these limits, which corresponds to the well-known Haken potential, consistently underestimates $\Delta E_B^{ab \text{ initio}}$, while the $q \rightarrow 0$ limit leads to a small overestimation. As introduced by Haken [23, 24] and also elaborated by Strinati [11], exciton coefficients in several semiconductors, are highly localized around $\mathbf{k} = \mathbf{0}$ in reciprocal space, motivating the $k \rightarrow 0$ approximation. However, this approximation also suggests that one may neglect the dispersion of electronic bands, only retaining the finite dispersion of the LO phonon. In materials such as the ones studied here, $A_{\mathbf{k}}$ assume appreciable non-zero values away from Γ , and this approximation is no longer valid, leading to the observed poor agreement between $\Delta E_B^{k \rightarrow 0}$ and $\Delta E_B^{ab \text{ initio}}$. For the systems investigated in this work, considering the momentum of phonons to be negligible compared to that of the electrons, *i.e.* taking the $q \rightarrow 0$ in the energy denominators of Eq. 19 and leading to the expression of Eq. 25, is physically better justified, leading to better agreement with first-principles

system	E_B	ω_{LO}	ϵ_∞	ϵ_0	$\Delta E_B^{ab\ initio}$	$\Delta E_B^{k \rightarrow 0}$ (Eq. 22)	$\Delta E_B^{q \rightarrow 0}$ (Eq. 25)	ΔE_B^{F-H} (Eq. 19)
GaN	65	87	5.9	10.8	-15	-6	-22	-15
AlN	143	110	4.5	8.7	-29	-16	-36	-29
MgO	327	84	3.3	11.3	-46	-26	-52	-48
CdS	39	34	6.2	10.4	-6	-3	-9	-6
SrTiO ₃	122	98	6.2	409	-44	-25	-65	-51

TABLE II. Comparison of the shift of the exciton binding energy at 0 K due to phonon screening in the different studied systems. All energy values are given in meV. For reference, the computed value of the exciton binding energy E_B as obtained from the solution of the bare BSE (without phonon effects) is given here, alongside the values computed within DFPT for the LO phonon frequency and the high-/low-frequency dielectric constants $\epsilon_{\infty,o}$.

calculations.

Moreover, the correction ΔE_B^{F-H} , obtained through numerical integration of Eq. 19, which only assumes hydrogenic excitons and an electron-phonon interaction governed by the Fröhlich vertex, is in excellent agreement with the first-principles results, for all systems but SrTiO₃, for reasons discussed in detail in Section IV C. For the remaining systems studied here, the hydrogenic and Fröhlich approximation are well-justified, as discussed in Ref. [25], leading to the excellent agreement between ΔE_B^{F-H} and $\Delta E_B^{ab\ initio}$.

C. First-principles calculations of finite temperature exciton binding energies and dissociation timescales

In what follows, we will employ the fully first-principles phonon kernel and focus on temperature-dependent effects of phonon screening on excitons, in three of the materials selected from Table II. Specifically, we focus on CdS, the material with lowest LO phonon frequency, which indicates the potential of this material for exhibiting substantial temperature-dependent phonon screening. Additionally, GaN is the only system studied here with $\omega_{LO} > E_B$, thus the absorption of an LO phonon from the exciton may lead to dissociation of the electron-hole pair, according to Eq. 16. Finally, we discuss the effects of phonon screening on the cubic perovskite phase of SrTiO₃, which has a very large ϵ_0 value, and is the only material showing significant deviations between the *ab initio* and ΔE_B^{F-H} corrections to the exciton binding energy at 0 K. In Appendix D we estimate the effects of thermal expansion on the phonon screening of excitons, which we generally find to be small. As also discussed in Appendix D, thermal expansion can cause a modest reduction of the exciton binding energy, additional to that caused by phonon screening, leading to overall improved agreement with experiment. Nevertheless, phonon screening remains the dominant effect that determines the temperature dependence of exciton binding energies.

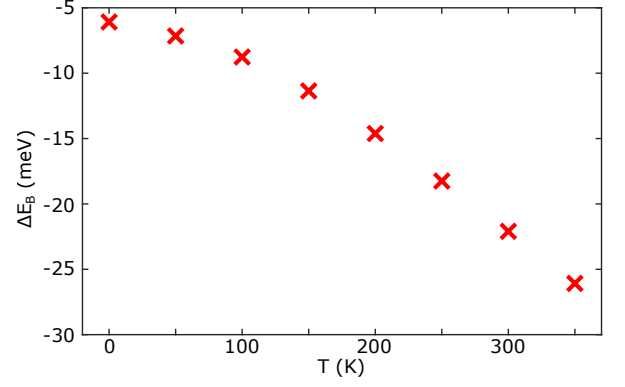


FIG. 2. Calculated shift of the exciton binding energy of CdS due to phonon screening, as a function of temperature.

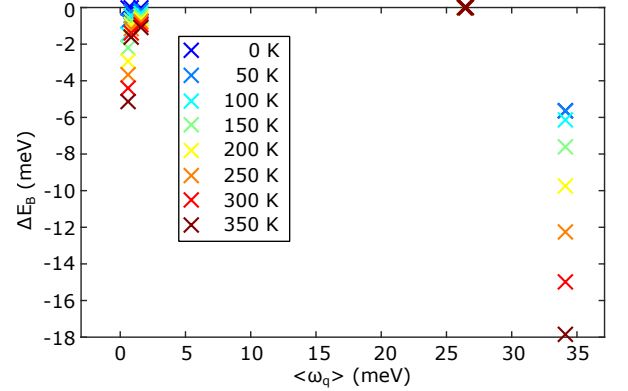


FIG. 3. Contribution of different phonon modes to the exciton binding energy shift of CdS due to phonon screening, as a function of temperature. Here $\langle \omega_q \rangle$ denotes the average frequency of a particular phonon branch.

1. CdS

In Fig. 2, we find that the correction of the exciton binding energy of CdS due to phonon screening is strongly temperature-dependent. The low-temperature correction is equal to almost -6 meV, and becomes more significant at room temperature, where it reaches a value of -22 meV. This suggests that the bare, clamped-ion exciton binding energy of CdS of 39 meV as computed from BSE (see Table II), will be renormalized by more than

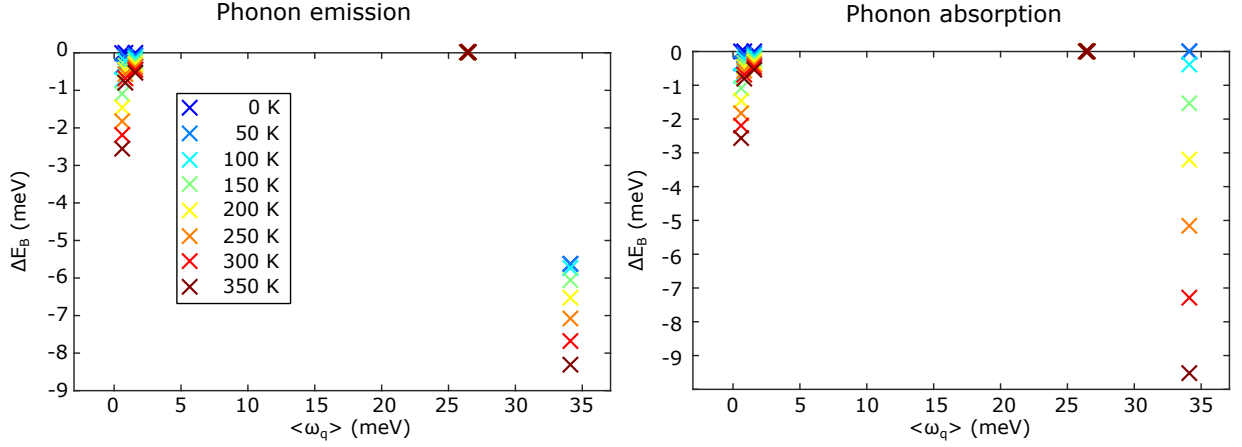


FIG. 4. Contribution of emission and absorption of different phonon modes to the exciton binding energy shift of CdS due to phonon screening, as a function of temperature. Here $\langle\omega_q\rangle$ denotes the average frequency of a particular phonon branch.

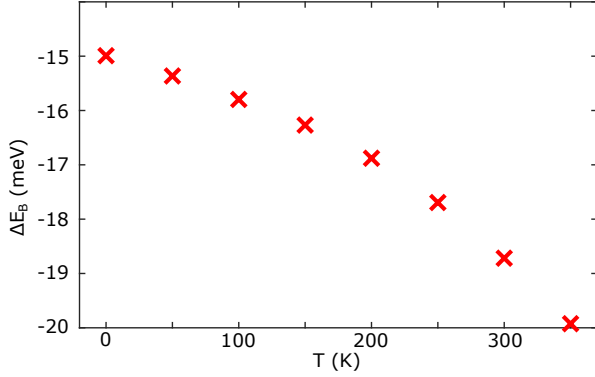


FIG. 5. Calculated shift of the exciton binding energy of GaN due to phonon screening, as a function of temperature.

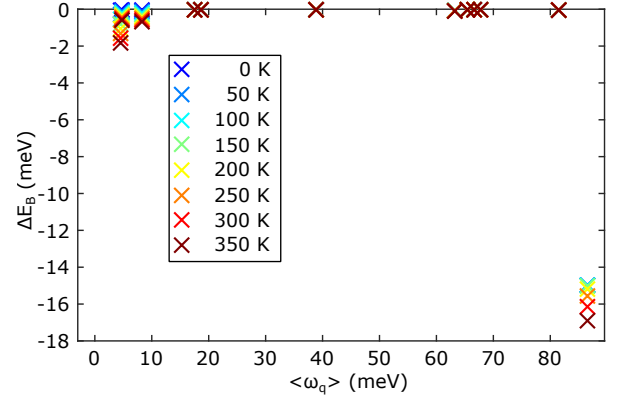


FIG. 6. Contribution of different phonon modes to the exciton binding energy shift of GaN due to phonon screening, as a function of temperature. Here $\langle\omega_q\rangle$ denotes the average frequency of a particular phonon branch.

50%, to 17 meV at 300 K, due to phonon screening. The experimental value for the exciton binding energy has been reported at low temperatures to be 28–30 meV [76–78], in good agreement with our low-temperature result of a corrected exciton binding energy of 33 meV. Experimental temperature-dependent studies of CdS excitons assume the exciton binding energy to be temperature-independent [78], and extract it as the activation energy of a fit of photoluminescence data. Our results show that through the phonon modification of the BSE kernel, the excitonic interactions become themselves temperature-dependent, resulting in the strong temperature dependence of the exciton binding energy of CdS shown in Fig. 2.

It is instructive to decompose the computed phonon-induced screening correction to the exciton binding energy into contributions from different phonon branches of CdS. As seen in Fig. 3, unsurprisingly the vast majority of this effect is driven by the LO phonon with an average frequency of 34 meV across the Brillouin zone. The contribution of this phonon to ΔE_B increases substantially with temperature, due to its low frequency and high

thermal activation. Interestingly, we also find that at finite temperatures there is a non-negligible contribution of acoustic phonons to the screening, which is strongly temperature-dependent due to the large thermal occupation factors of these modes. We return to the contribution of acoustic modes to phonon screening of excitons in Section V.

Eq. 9 allows us to identify the separate contributions of phonon absorption and emission to the phonon kernel. For CdS, we visualize in Fig. 4 the impact of these effects on the exciton binding energy. Notably, phonon emission is already active at low temperatures, while phonon absorption only provides a minor contribution. This is intuitive, as the relevant phonons are unavailable to be absorbed from the environment at low temperatures, according to Eq. 9. The precise temperature where phonons become available to be absorbed may also depend on the level of theory used to obtain phonon frequencies (for example on the exchange-correlation functional [79] or

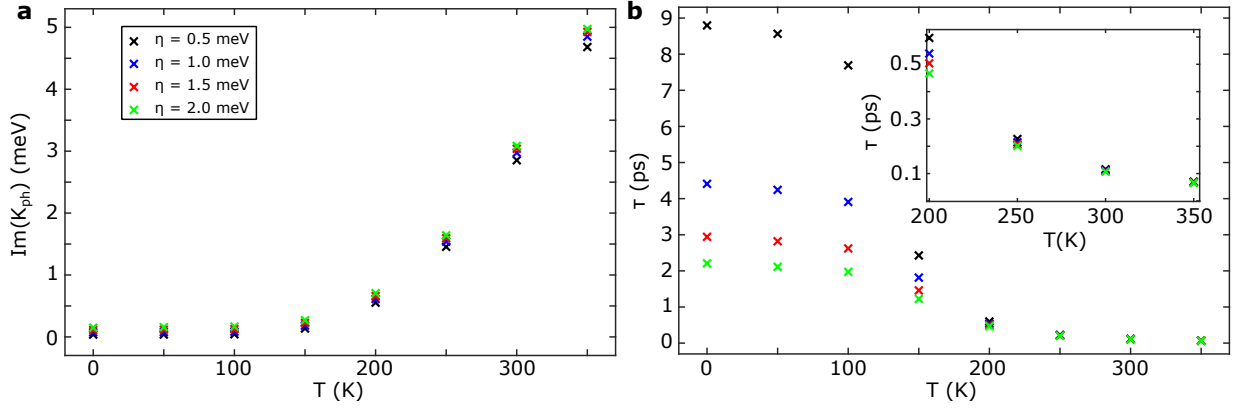


FIG. 7. Imaginary part of the phonon kernel matrix elements between the $1s$ exciton basis states (panel **a**) and associated calculated timescale for exciton dissociation (panel **b**) as a function of temperature and the η parameter for GaN. The inset of panel **b** provides a closer view of the range of temperatures around 300 K.

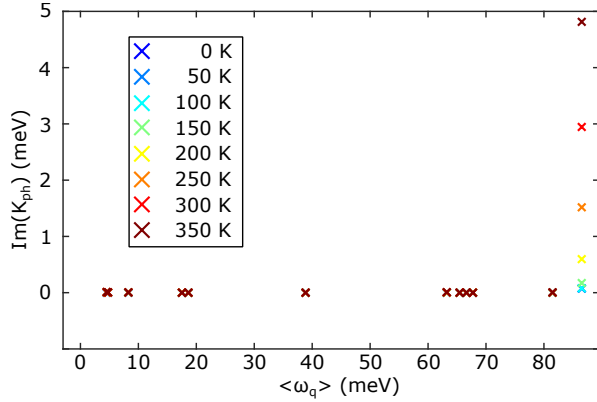


FIG. 8. Contribution of different phonon modes to the imaginary part of the phonon kernel of GaN, as a function of temperature and for $\eta = 1$ meV. Here $\langle\omega_q\rangle$ denotes the average frequency of a particular phonon branch.

the inclusion of anharmonic effects [80]). Despite this expected sensitivity, we expect the contribution of the absorption term to ΔE_B at small temperatures will be small. On the other hand, the phonon emission term survives even when $N_B(\omega_{q,\nu}, T) \rightarrow 0$, and indeed the 0 K results of Table II are entirely due to phonon emission. As the temperature increases, the contribution of phonon absorption to the screening of the exciton becomes more substantial, and eventually emission and absorption contribute equally.

2. GaN

The value of ΔE_B for GaN only shows weak temperature dependence as seen in Fig. 5, since the frequency of its LO phonon has a value of 84 meV, significantly above room temperature. As for CdS, ΔE_B is dominated by the LO phonon (see Fig. 6) while here too there is a small but non-negligible contribution from acoustic phonons.

Solution of the bare BSE gives an exciton binding energy of $E_B = 65$ meV for GaN, and by including the correction due to phonon screening we predict it will decrease to 46 meV at 300 K. The experimental values for the exciton binding energy of GaN are within the range of 20–28 meV [81, 82], with some studies measuring this quantity at room temperature [82] and others at cryogenic temperatures [81]. We were not able to find a systematic experimental study on the temperature dependence of the exciton binding energy; however, it is clear that while inclusion of phonon screening effects leads to better agreement with experiment, we still overestimate the exciton binding energy, similar to the case of the halide perovskites [25]. This result could be attributed to the fact that the magnitude of electron-phonon interaction within DFPT might be underestimated compared to using higher level theories [48, 83, 84], as well as to the fact that we do not account for polaronic interference effects as discussed in Section II A.

Among the systems studied in this work, GaN is the only one for which $\omega_{LO} > E_B$, making it a case where the absorption of a single LO phonon by the exciton might lead to its dissociation into a free electron-hole pair. The fact that $\omega_{LO} > E_B$ manifests as a finite value of $\text{Im}[K_{SS}^{ph}(\Omega_S, T)]$, as shown in Fig. 7a. The value of η in Eq. 9 represents a small arbitrary broadening we introduce to the energy levels appearing in the denominator, in order to resolve the crossing between an exciton that has absorbed a phonon, and the free electron-hole pair, as schematically shown in Fig. 1. Given the fine grid we are employing here ($100 \times 100 \times 100$) we find that values of η within the range of 0.5–2 meV are sufficient to satisfy this energy conservation condition. In Fig. 7a, we plot $\text{Im}[K_{SS}^{ph}(\Omega_S, T)]$ for a range of η values within that window and find that the change in the result is minor. Our values for $\text{Im}[K_{SS}^{ph}(\Omega_S, T)]$ are similar to the imaginary part of the self-energy of a model system [31], representing phonon-mediated exciton-exciton scattering, indicating that these effects are directly competing.

In Fig. 7b we plot the exciton dissociation timescale for the lowest singlet exciton of GaN using Eq. 16, as a function of temperature and for different values of η . This exciton dissociation process is entirely due to the absorption of LO phonons by the exciton, as no other phonons contribute to the imaginary part of the phonon kernel (see Fig. 8). We see from Fig. 7b that at low temperatures, the exciton dissociation timescale varies significantly with changes in the value of η . This is due to the fact that the imaginary part of the phonon kernel for temperatures up to approximately 150 K assumes very small values of less than 0.5 meV, making even small changes in η significant for its inverse in Eq. 16. Nevertheless the exciton dissociation timescale τ becomes more stable with respect to changes in the value of η at higher temperatures, as also highlighted in the inset of Fig. 7b. At 300 K we find $\tau = 111$ fs. While we have not found experimental studies on time-resolved exciton dissociation in GaN to compare against, it is encouraging that recent experiments employing ultrafast 2D electronic spectroscopy report exciton dissociation timescales that are similar to what we compute here, for semiconductors with comparable exciton binding energies. Specifically, for GaSe an exciton dissociation timescale of 112 fs at room temperature has been reported [85], while for $\text{CH}_3\text{NH}_3\text{PbI}_3$, an exciton dissociation timescale of approximately 50 fs [86] was found.

It is also worth pointing out that the finite exciton lifetime described by the imaginary part of the phonon kernel, will manifest as a finite linewidth in absorption and emission spectra. However, exciton dissociation will only be one of several scattering processes contributing to the overall linewidth observed in experiment, with phonon-mediated exciton-exciton scattering [40, 64], Auger recombination [87], and more, all contributing to the total linewidth. It is therefore no surprise that our value of approximately 3 meV for the imaginary part of the phonon kernel of GaN at 300 K is substantially smaller than the experimental linewidth of approximately 20 meV at the same temperature [88].

3. SrTiO_3

Among the systems of Table II, SrTiO_3 is the only one for which we find a substantial difference in the value of $\Delta E_B^{\text{F-H}}$ at 0 K as predicted from the numerical integration of Eq. 19, and the full *ab initio* correction $\Delta E_B^{ab \text{ initio}}$ to the exciton binding energy, following Eq. 9. Moreover, this is a system with a very large value for the low-frequency dielectric constant ϵ_0 , indicating a potentially very large contribution of phonons to the screened Coulomb interaction, making it particularly interesting for further study.

In Fig. 9 we visualize the temperature-dependent correction ΔE_B to the exciton binding energy for this system, which we find to be equal to -52 meV at 300 K, renormalizing the bare clamped-ion exciton binding en-

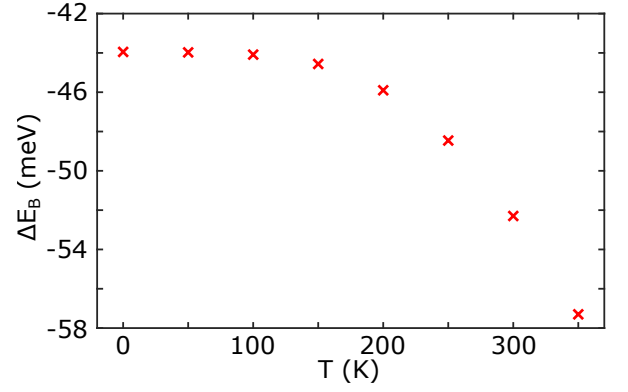


FIG. 9. Calculated shift of the exciton binding energy of SrTiO_3 due to phonon screening, as a function of temperature.

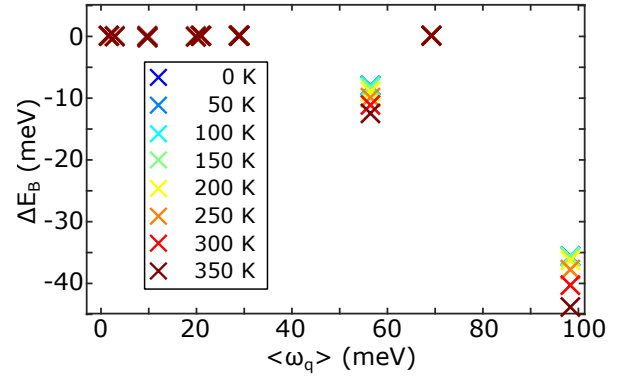


FIG. 10. Contribution of different phonon modes to the exciton binding energy shift of SrTiO_3 due to phonon screening, as a function of temperature. Here $\langle\omega_q\rangle$ denotes the average frequency of a particular phonon branch.

ergy as computed within BSE by 43%, from 122 meV to 70 meV. By decomposing this correction to the effect of individual phonons in Fig. 10, we find that while phonon screening in this system is dominated by the LO mode with a frequency of 98 meV (henceforth referred to as LO-1), there is a substantial contribution from an LO phonon with a lower frequency of 57 meV (henceforth referred to as LO-2), which has been discussed previously to also exhibit Fröhlich-like coupling [89].

The reason behind the disagreement of the *ab initio* and $\Delta E_B^{\text{F-H}}$ results for the correction to the exciton binding energy is that SrTiO_3 has multiple phonon modes contributing to the phonon screening and the static dielectric constant ϵ_0 . In these cases, the Fröhlich model, which is used in the numerical integration of Eq. 19, breaks down, and one needs to instead use the generalized Fröhlich vertex of Ref. [90]. For a phonon ν , this is written as

$$g_{\mathbf{q},\nu} = i \frac{4\pi}{V} \sum_j \left(\frac{1}{2NM_j\omega_{\mathbf{q},\nu}} \right)^{1/2} \cdot \frac{\mathbf{q} \cdot \mathbf{Z}_j \cdot \mathbf{e}_{j,\nu}(\mathbf{q})}{\mathbf{q} \cdot \epsilon_\infty \cdot \mathbf{q}}, \quad (26)$$

in atomic units. For atom j , \mathbf{Z}_j is its Born effective

phonon mode	$\Delta E_B^{\text{F-H}}$	$\Delta E_B^{\text{F-H, gen.}}$	$\Delta E_B^{ab \text{ initio}}$
LO-1	-51	-38	-36
LO-2	-34	-8	-8

TABLE III. Phonon-resolved screening of the exciton binding energy of SrTiO₃ by the two LO modes of this material at 0 K (in meV). We compare full *ab initio* level theory ($\Delta E_B^{ab \text{ initio}}$), the numerical integration of Eq. 19 using the standard Fröhlich vertex for each phonon ($\Delta E_B^{\text{F-H}}$), as well as the numerical integration of Eq. 19 employing the generalized Fröhlich vertex ($\Delta E_B^{\text{F-H, gen.}}$).

charge tensor and M_j its mass, while V the unit cell volume, N the number of unit cells, and $e_{j,\nu}(\mathbf{q})$ the phonon eigenvectors. In Table III we show that employing this generalized Fröhlich vertex in the numerical integration of Eq. 19 gives excellent agreement with the *ab initio* result for the correction to the exciton binding energy of SrTiO₃ due to its LO-1 and LO-2 phonons. On the other hand, numerically integrating Eq. 19 for the LO-1 and LO-2 phonons using the standard Fröhlich vertex of Eq. 17 leads to significant discrepancies with the *ab initio* results. The comparison between the case where we use the Fröhlich and hydrogenic approximations, and the *ab initio* result, is discussed in more detail in Appendix E.

D. Phonon screening from acoustic modes

As seen in the previous Section IV C, and specifically, in Figures 3 and 6, acoustic phonons can result in a substantial reduction of the exciton binding energy in CdS and GaN. Moreover, among the systems studied in this work, AlN is the only other case where acoustic phonons contribute to phonon screening. What these materials have in common is that all three are piezoelectric [91, 92], enabling a large coupling of the electrons with acoustic phonons [46], with the average electron-phonon coupling of acoustic modes scaling monotonically with the experimental piezoelectric constants, as seen in Fig. 11.

As shown previously, ignoring quadrupole terms in the Wannier-Fourier interpolation of the electron-phonon matrix elements of acoustic phonons can lead to an overestimation of the magnitude of g in the vicinity of Γ [93]. Therefore, it is possible that inclusion of quadrupole corrections will lead to a modest reduction of the predicted screening of the exciton binding energy by acoustic phonons. Nevertheless, the contribution of acoustic phonons to screening excitons will be important in piezoelectric materials, highlighting the importance of going beyond the simple picture within which optical phonons are the only ones contributing to this effect.

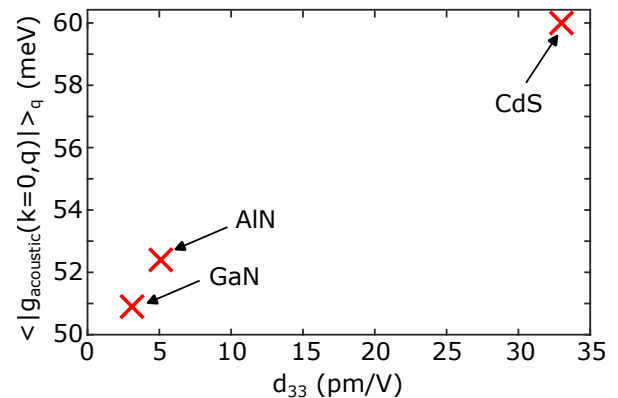


FIG. 11. Average electron-phonon coupling of acoustic modes of CdS, AlN and GaN, plotted against the experimental piezoelectric coefficient (Ref. [91] for AlN and GaN, Ref. [92] for CdS).

V. DISCUSSION, CONCLUSIONS AND OUTLOOK

In this work we have developed an *ab initio* framework for computing the temperature-dependent phonon kernel of semiconductors and insulators, according to Eq. 9. We show how approximations to the phonon kernel lead to the model expressions of Eq. 22, 25 and 19, some of which have been widely discussed in the literature. Compared to utilizing these model expressions, our *ab initio* approach does not rely on any restrictive approximations, treating the effect of all phonon modes on equal footing without any assumption about the nature of their coupling to electrons. It also allows us to extend our results to finite temperatures in a straightforward manner, and to go beyond the Wannier-Mott model, which will be critical in systems where excitons are not hydrogenic in nature [57]. Additionally, the imaginary part of the phonon kernel in the exciton basis allows us to extract information about temperature-dependent exciton dissociation processes in certain limits. Overall, having access to the full, temperature-dependent complex phonon kernel enhances our ability to predict excitonic properties while providing new physical insights, with some of the ones obtained in this work summarized below.

Firstly, we found that for bulk CdS, phonon screening reduces the bare BSE exciton binding energy by more than 50% at room temperature, demonstrating that the effect of phonon screening on excitons can be very strong and highly temperature-dependent. Our theoretical framework provides a temperature-dependent correction to the BSE kernel and therefore to the excitonic interactions. Indeed, experimental studies already in the 1970s and 1980s found indications of strongly temperature-dependent excitonic interactions, but were unable to quantify this effect [94–96]. These modified interactions can lead to strongly temperature-dependent exciton binding energies, as recent experimental studies have found [97, 98], and at odds with the common as-

sumption of a temperature-independent exciton binding energy [78, 88].

Our formalism describes the screening of the exciton due to both processes of emission and absorption of phonons, effects that contribute equally to the reduction of the exciton binding energy at 300 K, while phonon emission processes entirely dominate at low temperatures. Additionally, we found an important reduction of the exciton binding energy due to screening from acoustic phonons in piezoelectric materials, which, to the best of our knowledge, has not been previously discussed.

Importantly, having access to the imaginary part of the phonon kernel allows us to compute exciton dissociation rates via single-phonon emission and absorption processes entirely from first principles. For the case of GaN where $E_B < \omega_{LO}$, the absorption of a LO phonon is sufficient to dissociate the exciton and generate a free electron-hole pair. Our computed exciton dissociation timescale for this system is approximately 111 fs at 300 K. While we have not found experimental exciton dissociation timescales for GaN to compare against, it is encouraging that our predicted value is reasonably close to experimental values obtained in semiconductors with comparable exciton binding energies, such as GaSe with an exciton dissociation timescale of 112 fs [85], and $\text{CH}_3\text{NH}_3\text{PbI}_3$ with an exciton dissociation timescale of approximately 50 fs [86].

Moving forward, our first-principles approach could be extended in multiple ways. For example, one could resolve the BSE non-perturbatively upon correction of the electronic BSE kernel, which might substantially change the exciton wavefunction and computed absorption spectra for systems where the phonon kernel in the bare exciton basis has large off-diagonal entries. Furthermore, one could consider the interplay of phonon screening with the effects of polaronic mass enhancement and polaron interference on excitons [19, 20] by incorporating higher-order diagrams into this approach. Our approach for ensuring gauge consistency between interpolated electron-phonon matrix elements and exciton coefficients could be extended to account for the effects of phonon screening and other diagrams on finite-momentum excitons [31], by utilizing recent schemes for exciton Wannier functions [99]. While in this work we have studied some representative semiconducting materials, we hope our first-principles approach will be widely adopted and used to study the effect of phonons on dissociating and screening excitons in diverse materials of interest for a variety of technological applications, such as heterostructures of two-dimensional semiconductors, quantum wells, or doped systems.

ACKNOWLEDGMENTS

This work was primarily supported by the Theory FWP, which provided *GW* and *GW*-BSE calculations and analysis of phonon effects, and the Center for Computational Study of Excited-State Phenomena in En-

ergy Materials (C2SEPPEM) as part of the Computational Materials Sciences Program, which provided advanced codes, at the Lawrence Berkeley National Laboratory, funded by the U.S. Department of Energy, Office of Science, Basic Energy Sciences, Materials Sciences and Engineering Division, under Contract No. DE-AC02-05CH11231. Z.L. and S.G.L. acknowledge support from the National Science Foundation under Grant No. OAC-2103991 in the development of interoperable software enabling the EPW and BerkeleyGW calculations with consistent gauge. Computational resources were provided by the National Energy Research Scientific Computing Center (NERSC). M.R.F. acknowledges support from the UK Engineering and Physical Sciences Research Council (EPSRC), Grant EP/V010840/1.

Appendix A: Estimated exciton and polaron radii of studied systems

Table IV summarizes the exciton Bohr radius a_o and the electron-/hole-polaron radii $r_{e,h}$ of the studied systems. The exciton bohr radius is estimated as $a_o = 1/(2E_B\mu)^{1/2}$ within the Wannier-Mott model, where E_B the converged BSE exciton binding energies given in Table II, and μ the exciton effective mass $1/\mu = 1/m_e + 1/m_h$, with m_e and m_h the effective mass of the electron and hole, respectively. A more quantitatively accurate calculation of the exciton radius would require using first-principles methods that accurately capture this quantity [100]. The estimated electron-/hole-polaron radii are obtained as $r_{e,h} = \frac{1}{\sqrt{2m_{e,h}\omega_{LO}}}$ [20], under the assumption of weak, Fröhlich-like electron-phonon coupling. While recent development of first-principles methodologies now allows more accurate computation of the spatial extent of electron and hole polarons [101], the values reported in Table IV indicate that our studied materials are within the regime where the lattice polarization associated with the two polarons may interfere significantly, as described elsewhere [19, 42].

Moreover, Table IV summarizes the electron and hole effective masses. We compute the effective masses for the top/bottom of the valence and conduction bands respectively using the finite difference formula $\frac{1}{m^*} = \frac{E(\delta\mathbf{k}) + E(-\delta\mathbf{k}) - 2E(\Gamma)}{\delta\mathbf{k}^2}$, taking $\delta\mathbf{k}$ to be equal to 0.01 (in crystal coordinates) along each spatial direction, and we average over the three spatial directions. The energies E are computed at the *GW* level.

Appendix B: Imaginary part of the phonon kernel as an exciton dissociation rate

Here we outline in greater detail the arguments, using scattering theory and many-body perturbation theory techniques [46, 58], that establish the imaginary part of the diagonal elements of the phonon kernel in the un-

Material	m_e (a.u.)	m_h (a.u.)	a_o (Å)	r_e (Å)	r_h (Å)
AlN	0.30	0.70	11.3	10.8	7.0
CdS	0.12	2.01	29.4	30.5	7.5
GaN	0.15	1.01	21.1	17.3	6.7
MgO	0.34	5.00	6.1	11.6	3.0
SrTiO ₃	0.39	1.22	10.2	9.9	5.6

TABLE IV. Estimated exciton Bohr radii a_o , electron-/hole-polaron radii $r_{e,h}$, and electron/hole effective masses $m_{e,h}$ of the studied systems.

perturbed exciton basis as related to the rate of the dissociation channel for excitons into free electron-hole pairs, due to the absorption of a single phonon.

Within the GW -BSE formalism and accounting for phonon screening, the dynamics of a system of excitons and phonons is described by the Hamiltonian

$$H = (E_{c\mathbf{k}} - E_{v\mathbf{k}})\delta_{vv'}\delta_{cc'}\delta_{\mathbf{k}\mathbf{k}'} + K_{cv\mathbf{k},c'v'\mathbf{k}'}^{eh} + H_{ph} + K_{cv\mathbf{k},c'v'\mathbf{k}'}^{ph}, \quad (\text{B1})$$

where H_{ph} is the phonon Hamiltonian and $H_{\text{BSE}} = (E_{c\mathbf{k}} - E_{v\mathbf{k}})\delta_{vv'}\delta_{cc'}\delta_{\mathbf{k}\mathbf{k}'} + K_{cv\mathbf{k},c'v'\mathbf{k}'}^{eh}$ is the usual bare BSE Hamiltonian.

At temperature T the initial (bare exciton) state of Fig. 1 is a particular eigenstate of the Hamiltonian $H_i = H_{\text{BSE}} + H_{ph}$:

$$H_i |S, N_B + 1\rangle = E_i^S |S, N_B + 1\rangle, \quad (\text{B2})$$

with energy $E_i^S = \Omega_S + (N_B + 1)\omega_{LO}$. We consider here the example of an LO phonon with occupation N_B at temperature T , but the same holds for any phonon mode. The absorption of a single phonon can lead to a final (free electron-hole) state, which also can be expressed as an eigenstate of the distinct but related Hamiltonian $H_f = (E_{c\mathbf{k}} - E_{v\mathbf{k}})\delta_{vv'}\delta_{cc'}\delta_{\mathbf{k}\mathbf{k}'} + H_{ph}$, where

$$H_f |(\mathbf{c}\mathbf{k}, \mathbf{v}\mathbf{k}'), N_B\rangle = E_f |(\mathbf{c}\mathbf{k}, \mathbf{v}\mathbf{k}'), N_B\rangle, \quad (\text{B3})$$

with $E_f = E_{c\mathbf{k}} - E_{v\mathbf{k}'} + N_B\omega_{LO}$. The initial and final states are described as eigenstates of different Hamiltonians, apparently complicating a straightforward interpretation of the scattering process, as one needs to ensure orthogonality between these wavefunctions [60]. However, this complication is resolved using the arguments of the theory of rearrangement collisions [61–63]. We can define a renormalized final free electron-hole state $|\chi_f\rangle$, which satisfies orthogonality to the initial state $|S, N_B + 1\rangle$, as [64]

$$|\chi_f\rangle = |(\mathbf{c}\mathbf{k}, \mathbf{v}\mathbf{k}'), N_B\rangle + (E_f - H - i\eta)^{-1} K^{eh} |(\mathbf{c}\mathbf{k}, \mathbf{v}\mathbf{k}'), N_B\rangle. \quad (\text{B4})$$

State $|\chi_f\rangle$ may be used to define a generalized \mathcal{S} -matrix for the scattering process, which to first order in the electron-phonon interaction and within the Born approx-

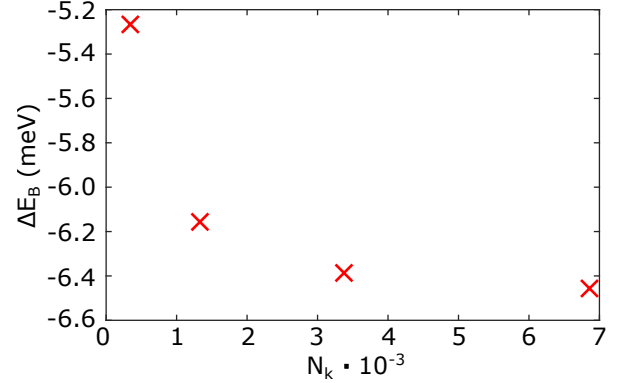


FIG. 12. Convergence of the exciton binding energy shift of CdS due to phonon screening at 0 K, with respect to the number of k-points in a patch centered around the Γ -point of a $100 \times 100 \times 100$ grid.

imation is written as

$$\mathcal{S}_{gen}^{Born} = 2\pi i \delta(E_f - E_i) \langle (\mathbf{c}\mathbf{k}, \mathbf{v}\mathbf{k}'), N_B | K^{ph} | S, N_B + 1 \rangle. \quad (\text{B5})$$

Employing the optical theorem for this \mathcal{S} -matrix in standard fashion, $\text{Im}[K_{SS}^{ph}(\Omega_S, T)]$ can be interpreted as the rate of this exciton dissociation process, namely

$$2|\text{Im}[K_{SS}^{ph}(\Omega_S, T)]| \approx \tau_S^{-1}(T). \quad (\text{B6})$$

Appendix C: Convergence of the first-principles phonon kernel

Figures 12 and 13 demonstrate the convergence of the real part of K^{ph} in CdS and GaN respectively, *i.e.* the correction ΔE_B to their exciton binding energy from phonons. By employing a patch taken from a $100 \times 100 \times 100$ regular grid, we are able to demonstrate convergence within less than 1 meV at 0 K, for a patch cutoff of 0.09 (in crystal coordinates) around Γ , corresponding to 6,859 \mathbf{k}/\mathbf{q} -points.

For SrTiO₃ convergence is more challenging to achieve. Fig. 14 demonstrates the values of $\Delta E_{B,gen}^{F-H}$ contributed by the LO-1 phonon, as predicted by Eq. 19 when using the generalized Fröhlich vertex of Eq. 26. In order to fully converge ΔE_B we have to compute the sum of Eq. 19 on a grid of 29,791 \mathbf{k}/\mathbf{q} -points (corresponding to a patch with a cutoff of 0.15 around Γ in crystal coordi-

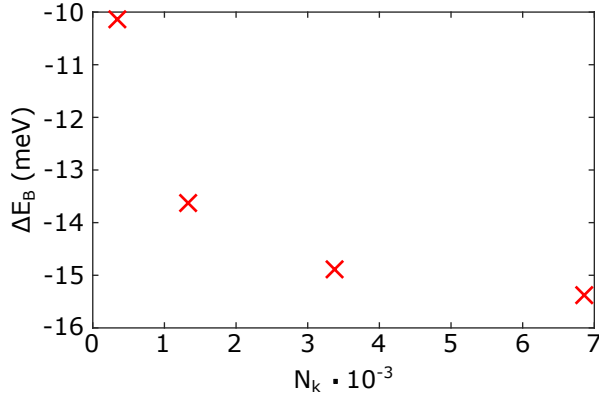


FIG. 13. Convergence of the exciton binding energy shift of GaN due to phonon screening at 0 K, with respect to the number of k-points in a patch centered around the Γ -point of a $100 \times 100 \times 100$ grid.

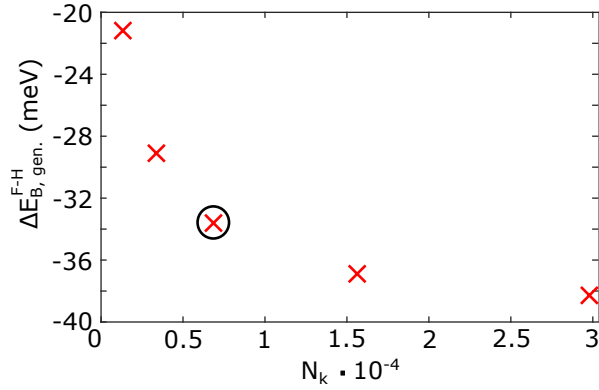


FIG. 14. Convergence of the exciton binding energy shift of SrTiO₃ due to phonon screening from the LO-1 mode at 0 K, with respect to the number of k-points in a patch centered around the Γ -point of a $100 \times 100 \times 100$ grid, as computed through numerical integration of the approximate Eq. 19 employing the generalized Fröhlich vertex of Eq. 26. The point in the black circle corresponds to the maximum grid size which was accessible through our *ab initio* workflow, and which is extrapolated to the $N_k \rightarrow \infty$ limit as discussed in the text.

nates, drawn from a $100 \times 100 \times 100$ regular grid), which is possible to do within this numerical integration employing the hydrogenic and Fröhlich formulas. However, convergence at the same level is very challenging to achieve from first principles. When employing our *ab initio* workflow, we were able to compute the phonon kernel on a Γ -centered patch with a cutoff of 0.09 (crystal coordinates), which includes 6,859 \mathbf{k}/\mathbf{q} -points, obtaining ΔE_B values of -31.1 meV and -7 meV for the LO-1 and LO-2 phonons respectively. For the same grid size, the numerical integration of Eq. 19 gives corrections of -33.6 meV and -7 meV for these two phonons respectively. Therefore, for the LO-2 phonon the two levels of theory are in perfect agreement at 0 K, whereas for the LO-1 phonon, the first-principles workflow gives a correction which is equal to 92.7% of the $\Delta E_B^{\text{F-H, gen.}}$ value of Fig. 14 on the

same grid size (circled in black). Consequently, in order to estimate the *ab initio* values at the $N_k \rightarrow \infty$ limit, for the LO-1 phonon contribution to $\Delta E_B^{\text{ab initio}}$, we take 92.7% of the converged value of $\Delta E_B^{\text{F-H, gen.}}$ as estimated from Eq. 19 (-38 meV), which is equal to -35 meV (Table III). For the LO-2 phonon the *ab initio* and the generalized Fröhlich-hydrogenic results on the patch of 6,859 \mathbf{k}/\mathbf{q} -points are identical, we therefore simply extrapolate the first-principles contribution to ΔE_B from this phonon from the slightly under-converged value of -7 meV, to the $N_k \rightarrow \infty$ limit of -8 meV. This same method for extrapolating to $N_k \rightarrow \infty$ is used for the phonon screening of the MgO exciton by the LO phonon of this material.

Appendix D: Effect of thermal expansion

In Table V we report the coefficients of linear thermal expansion of the systems we study here, as found in the literature. For SrTiO₃ we take a representative value for room temperature as reported for the zero external pressure case in Ref. [106]. Assuming linear thermal expansion over the temperature range 0 – 300 K, we estimate the percentage of change $\Delta a/a$ to the lattice constant over these temperatures for each material. We see in Table V that for AlN, CdS, and GaN, the lattice constants change by at most 0.2%, we therefore neglect this effect for the range of temperatures we are concerned with here. For MgO and SrTiO₃ there is a more significant change of approximately 1% to the lattice constant. For these two materials we have repeated the calculations of the bare and phonon-screened exciton binding energy, in order to evaluate the importance of thermal expansion.

Starting with MgO, expanding its lattice constant by 1% decreases the bare exciton binding energy of this system to 305 meV, compared to the 327 meV value of Table II. The LO phonon frequency also decreases from 84 meV to 81 meV. However, the *ab initio* phonon screening of the exciton remains almost unchanged, with the effect reduced by a mere 0.5 meV compared to the value of Table II.

For SrTiO₃, upon expansion of the lattice by 1%, the bare exciton binding energy reduces from 122 meV to 107 meV, while the LO-1 phonon also reduces its energy from 98 meV to 94 meV. While we were not able to obtain fully first-principles values for the phonon screening of the exciton of SrTiO₃ at this modified configuration due to the emergence of imaginary phonons, taking the $\mathbf{q} \rightarrow \mathbf{0}$ limit and using the model of Eq. 25, we obtain $\Delta E_B^{\mathbf{q} \rightarrow \mathbf{0}} = -61$ meV, compared to $\Delta E_B^{\mathbf{q} \rightarrow \mathbf{0}} = -65$ meV when not accounting for thermal expansion, which suggests a 6% decrease in the effect of phonon screening on the exciton binding energy.

Overall, we find that the effect of thermal expansion can lead to a small decrease of the screening of the exciton from phonons. This change in phonon screening is generally modest due to the fact that *both* ω_{LO} and E_B are reduced upon expansion of the lattice, making the change

Material	Thermal Expansion Coefficient (K^{-1})	Reference	$\Delta a/a(\Delta T = 300 \text{ K})$ (%)
AlN	$6.9 \cdot 10^{-6}$	[102]	0.2
CdS	$4.5 \cdot 10^{-6}$	[103]	0.14
GaN	$6 \cdot 10^{-6}$	[104]	0.18
MgO	$3.2 \cdot 10^{-5}$	[105]	1
SrTiO ₃	$3 \cdot 10^{-5}$	[106]	0.9

TABLE V. Thermal expansion coefficients of the studied systems, as found in the literature, and percentage of change to the a lattice constant assuming linear thermal expansion over 300 K.

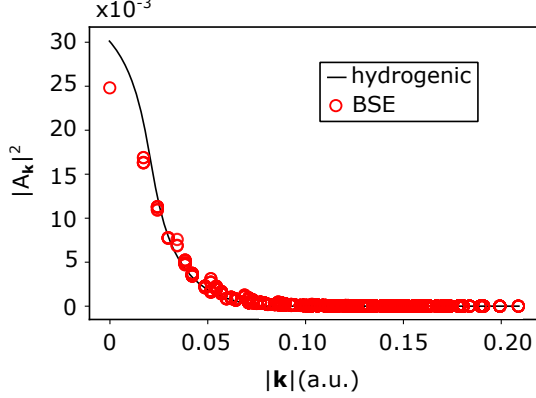


FIG. 15. Comparison of the exciton wavefunction in reciprocal space computed within *ab initio* GW-BSE and the hydrogenic model for SrTiO₃.

$\omega_{m,\mathbf{q}=0}$ (meV)	$\Delta\epsilon_m$
20	391.08
57	9.68
98	2.18

TABLE VI. Phonons with finite contributions to the static dielectric constant ϵ_0 of SrTiO₃.

in their ratio less significant. The reduction of the exciton binding energy due to thermal expansion, combined with the small effect of thermal expansion on phonon screening, will result to an overall larger decrease of exciton binding energies when thermal expansion and phonon screening are accounted for concurrently, and lead to better agreement with experimental values. Nevertheless, the temperature-dependent reduction of exciton binding energies due to phonon screening remains the dominant effect, as seen here even for MgO and SrTiO₃, the systems with the greatest effect of thermal expansion among the studied ones.

Appendix E: Comparison of Fröhlich-hydrogenic approximations to ΔE_B to fully *ab initio* values in SrTiO₃

The model of Eq. 19 only includes the effect of the highest frequency LO phonon, of 98 meV. One could therefore expect that comparing the value of ΔE_B obtained

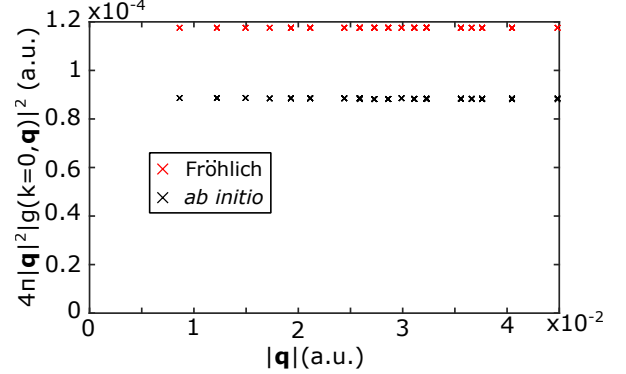


FIG. 16. Comparison of the *ab initio* and Fröhlich electron-phonon coupling g of SrTiO₃.

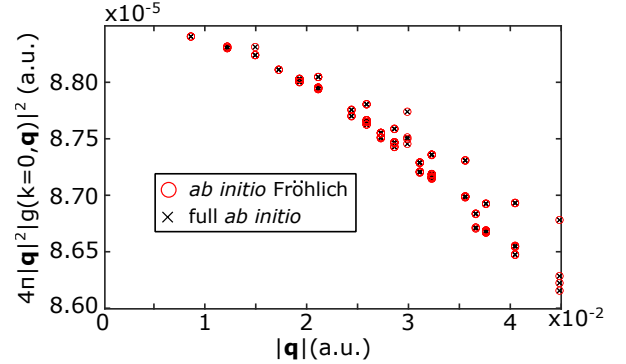


FIG. 17. Comparison of the *ab initio* long-range Fröhlich coupling g of Ref. [90] and the full *ab initio* electron-phonon coupling of SrTiO₃ for the LO-1 phonon.

through the numerical integration of Eq. 19 (-51 meV) to the *ab initio* value which is just due to the highest frequency LO phonon (-36 meV at 0 K) might improve agreement, but in fact it only makes the agreement between the two worse. The derivation of Eq. 19 from the full expression of Eq. 9, relies on two approximations. Specifically, excitons are assumed to be hydrogenic as described within the Wannier-Mott picture, and the electron-phonon interaction is considered to be entirely dominated by the long-range Fröhlich coupling of electrons to LO phonons. Therefore, at least one of these two approximation has to be violated for this system in order to explain the discrepancy between the Fröhlich-hydrogenic $\Delta E_B^{\text{F-H}}$ and first-principles $\Delta E_B^{\text{ab initio}}$ values

of Table II.

We first examine the validity of the hydrogenic model in SrTiO_3 . In Fig. 15 we compare the exciton wavefunction as computed within the BSE to the hydrogenic model described by Eq. 18, on a Γ -centered patch with a cutoff of 0.15 (in crystal coordinates), which is necessary to satisfy the normalization of the wavefunction within 1%. We see that the two are in good agreement, with some small deviations close to the zone center.

We now move to examine the agreement between the first-principles electron-phonon matrix elements g , and those predicted by the Fröhlich model g_{Fr} , for the LO-1 phonon, in Fig. 16, for a small region close to Γ . It is immediately apparent that the Fröhlich model consistently overestimates the first-principles values for the electron-phonon matrix elements, with the ratio $\frac{g_{Fr}^2}{g^2}$ equal to approximately 4/3. Since the correction to the exciton binding energy is proportional to $|g_{\mathbf{q}\nu}|^2$ it is reasonable to expect a similar overestimation, compared to the *ab initio* value. Indeed, if we naively multiply the first-principles value of -36 meV for the LO-1 phonon by 4/3 we get $\Delta E_B = -48$ meV, in very close agreement to the value of -51 meV predicted by the numerical integration of Eq. 19. Therefore most of the discrepancy can be attributed to the deviations of the Fröhlich vertex from its *ab initio* value, with the remaining difference likely due to the small differences between the hydrogenic and BSE exciton wavefunctions, see Fig. 15.

We now examine the reason behind this observed failure of the Fröhlich model. Unlike other systems studied here and presented in Table II, SrTiO_3 is the only material with more than a single LO phonon contributing to phonon screening, as seen in Fig. 10, as well as the only system among the studied ones where more than a single phonon mode m contributes to the low-frequency dielectric constant ϵ_0 . Following Ref. [107] we decompose ϵ_0 as $\epsilon_0 = \epsilon_\infty + \sum_m \Delta\epsilon_m$, and the phonon modes

m with finite $\Delta\epsilon_m$ contribution are given in Table VI, as computed from DFPT. The largest contribution to ϵ_0 comes from the soft polar mode with a frequency of 20 meV at Γ . This phonon does not contribute to the phonon screening of the exciton binding energy, due to its weak electron-phonon coupling around Γ [89], where the exciton coefficients are finite, and also because of its significantly lower energy compared to the exciton binding energy of 122 meV.

This large contribution to ϵ_0 by a phonon that ultimately does not contribute to phonon screening suggests that using ϵ_0 to estimate the Fröhlich coupling of the LO-1 and LO-2 modes will lead to an overestimation of the vertex g compared to a full first-principles calculation, as indeed we found in Fig. 16. The standard Fröhlich vertex was generalized in Ref. [90] to describe long-range electron-phonon interactions in anisotropic materials and within a mode-resolved picture for each phonon, as given in Eq. 26. This so-called *ab initio* Fröhlich vertex, perfectly reproduces the full first-principles values of the electron-phonon matrix elements close to $\mathbf{q} = \mathbf{0}$, as shown in Fig. 17 for the LO-1 phonon, and the same being true for the LO-2 phonon. This suggests that using Eq. 26 to describe the electron-phonon matrix element in Eq. 19 will restore good agreement between the first-principles $\Delta E_B^{ab initio}$ and numerically-integrated value of $\Delta E_{B,gen}^{F-H}$, with the latter now based on the hydrogenic model for excitons and the *generalized* Fröhlich model. Indeed in Table III we show that by applying these two levels of theory to the phonon modes LO-1 and LO-2, we recover close-to-perfect agreement between the results of Eq. 19 and taking the real part of Eq. 9. Any remaining discrepancy is attributed to the differences between the hydrogenic model and BSE in terms of describing the exciton wavefunction, see Fig. 15.

-
- [1] G. Grancini, M. Maiuri, D. Fazzi, A. Petrozza, H. J. Egelhaaf, D. Brida, G. Cerullo, and G. Lanzani, Hot exciton dissociation in polymer solar cells, *Nature Materials* **12**, 29 (2013).
 - [2] T. J. Savenije, C. S. Ponseca, L. Kunneman, M. Abdellah, K. Zheng, Y. Tian, Q. Zhu, S. E. Canton, I. G. Scherblykin, T. Pullerits, A. Yartsev, and V. Sundström, Thermally activated exciton dissociation and recombination control the carrier dynamics in organometal halide perovskite, *Journal of Physical Chemistry Letters* **5**, 2189 (2014).
 - [3] X. Ai, E. W. Evans, S. Dong, A. J. Gillett, H. Guo, Y. Chen, T. J. Hele, R. H. Friend, and F. Li, Efficient radical-based light-emitting diodes with doublet emission, *Nature* **563**, 536 (2018).
 - [4] S. Reineke, F. Lindner, G. Schwartz, N. Seidler, K. Walzer, B. Lüssem, and K. Leo, White organic light-emitting diodes with fluorescent tube efficiency, *Nature* **459**, 234 (2009).
 - [5] L. Hedin, New Method for Calculating the One-Particle Green's Function with Application to the Electron-Gas Problem, *Physical Review* **139**, 796 (1965).
 - [6] M. S. Hybertsen and S. G. Louie, Electron correlation in semiconductors and insulators: Band gaps and quasiparticle energies, *Physical Review B* **34**, 5390 (1986).
 - [7] S. Albrecht, L. Reining, R. Del Sole, and G. Onida, Ab initio calculation of excitonic effects in the optical spectra of semiconductors, *Phys. Rev. Lett.* **80**, 4510 (1998).
 - [8] L. X. Benedict, E. L. Shirley, and R. B. Bohn, Optical absorption of insulators and the electron-hole interaction: An ab initio calculation, *Physical Review Letters* **80**, 4514 (1998).
 - [9] M. Rohlfing and S. G. Louie, Electron-hole excitations in semiconductors and insulators, *Physical Review Letters* **81**, 2312 (1998).

- [10] M. Rohlfing and S. G. Louie, Electron-hole excitations and optical spectra from first principles, *Physical Review B - Condensed Matter and Materials Physics* **62**, 4927 (2000), 0406203v3 [arXiv:cond-mat].
- [11] G. Strinati, Application of the Green's functions method to the study of the optical properties of semiconductors, *La Rivista Del Nuovo Cimento Series 3* **11**, 1 (1988).
- [12] D. M. Ceperley and B. J. Alder, Ground state of the electron gas by a stochastic method, *Physical Review Letters* **45**, 566 (1980).
- [13] M. Bokdam, T. Sander, A. Stroppa, S. Picozzi, D. D. Sarma, C. Franchini, and G. Kresse, Role of Polar Phonons in the Photo Excited State of Metal Halide Perovskites, *Scientific Reports* **6**, 1 (2016), 1512.05593.
- [14] F. Bechstedt and J. Furthmüller, Influence of screening dynamics on excitons in Ga2O3 polymorphs, *Applied Physics Letters* **114**, 6 (2019).
- [15] P. Umari, E. Mosconi, and F. De Angelis, Infrared Dielectric Screening Determines the Low Exciton Binding Energy of Metal-Halide Perovskites, *Journal of Physical Chemistry Letters* **9**, 620 (2018).
- [16] A. Schleife, M. D. Neumann, N. Esser, Z. Galazka, A. Gottwald, J. Nixdorf, R. Goldhahn, and M. Feneberg, Optical properties of In2O3 from experiment and first-principles theory: Influence of lattice screening, *New Journal of Physics* **20**, 10.1088/1367-2630/aabee0 (2018).
- [17] F. Fuchs, C. Rödl, A. Schleife, and F. Bechstedt, Efficient O(N²) approach to solve the Bethe-Salpeter equation for excitonic bound states, *Physical Review B - Condensed Matter and Materials Physics* **78**, 1 (2008).
- [18] Y. Park and D. T. Limmer, Renormalization of excitonic properties by polar phonons, *Journal of Chemical Physics* **157**, 10.1063/5.0100738 (2022).
- [19] S. D. Mahanti and C. M. Varma, Effective electron an hole interactions in a polarizable field, *Physical Review Letters* **25**, 1115 (1970).
- [20] S. D. Mahanti and C. M. Varma, Effective Electron-Hole Interactions in Polar Semiconductors, *Physical Review B* **6**, 2209 (1972).
- [21] L. M. Herz, How Lattice Dynamics Moderate the Electronic Properties of Metal-Halide Perovskites, *Journal of Physical Chemistry Letters* **9**, 6853 (2018).
- [22] L. Adamska and P. Umari, Bethe-Salpeter equation approach with electron-phonon coupling for exciton binding energies, *Physical Review B* **103**, 75201 (2021).
- [23] H. Haken, Zur Quantentheorie des Mehrelektronensystems im schwingenden Gitter. I, *Zeitschrift für Physik* **146** (1956).
- [24] H. Haken, Die Theorie des Exzitons im festen Körper, *Fortschritte der Physik* **6** (1958).
- [25] M. R. Filip, J. B. Haber, and J. B. Neaton, Phonon Screening of Excitons in Semiconductors: Halide Perovskites and beyond, *Physical Review Letters* **127**, 67401 (2021), 2106.08697.
- [26] G. Baym, Field-theoretic approach to the properties of the solid state, *Annals of Physics* **14**, 10.1006/aphy.2000.6009 (1961).
- [27] L. Hedin, New Method for Calculating the One-Particle Green's Function with Application to the Electron-Gas Problem, *Physical Review* **139**, 796 (1965).
- [28] F. Giustino, Electron-phonon interactions from first principles, *Reviews of Modern Physics* **89**, 1 (2017).
- [29] L. Hedin and S. Lundqvist, Effects of Electron-Electron and Electron-Phonon Interactions on the One-Electron States of Solids, *Solid State Physics - Advances in Research and Applications* **23**, 1 (1970).
- [30] P. Cudazzo, First-principles description of the exciton-phonon interaction: A cumulant approach, *Physical Review B* **102**, 1 (2020).
- [31] G. Antonius and S. G. Louie, Theory of exciton-phonon coupling, *Physical Review B* **105**, 85111 (2022), 1705.04245.
- [32] F. Paleari and A. Marini, Exciton-phonon interaction calls for a revision of the "exciton" concept, *Physical Review B* **106**, 1 (2022), 2205.02783.
- [33] Y. Toyozawa, Theory of Line-Shapes of the Exciton Absorption Bands, *Progress of Theoretical Physics* **20**, 53 (1958).
- [34] F. Paleari, H. P. Miranda, A. Molina-Sánchez, and L. Wirtz, Exciton-Phonon Coupling in the Ultraviolet Absorption and Emission Spectra of Bulk Hexagonal Boron Nitride, *Physical Review Letters* **122**, 187401 (2019), arXiv:1810.08976.
- [35] E. Cannuccia, B. Monserrat, and C. Attaccalite, Theory of phonon-assisted luminescence in solids: Application to hexagonal boron nitride, *Physical Review B* **99**, 1 (2019).
- [36] P. Lechiffart, F. Paleari, D. Sangalli, and C. Attaccalite, First-principles study of luminescence in hexagonal boron nitride single layer: Exciton-phonon coupling and the role of substrate, *Physical Review Materials* **7**, 24006 (2023), arXiv:2212.10407.
- [37] A. M. Alvertis, J. B. Haber, E. A. Engel, S. Sharifzadeh, and J. B. Neaton, Phonon-Induced Localization of Excitons in Molecular Crystals from First Principles, *Physical Review Letters* **130**, 86401 (2023), arXiv:2301.11944.
- [38] A. M. Alvertis, R. Pandya, L. A. Muscarella, N. Sawhney, M. Nguyen, B. Ehrler, A. Rao, R. H. Friend, A. W. Chin, and B. Monserrat, Impact of exciton delocalization on exciton-vibration interactions in organic semiconductors, *Physical Review B - Condensed Matter and Materials Physics* **102**, 081122(R) (2020), arXiv:2006.03604.
- [39] H.-Y. Chen, D. Sangalli, and M. Bernardi, Exciton-Phonon Interaction and Relaxation Times from First Principles, *Physical Review Letters* **125**, 107401 (2020), 2002.08913.
- [40] Y. H. Chan, J. B. Haber, M. H. Naik, J. B. Neaton, D. Y. Qiu, F. H. da Jornada, and S. G. Louie, Exciton Lifetime and Optical Line Width Profile via Exciton-Phonon Interactions: Theory and First-Principles Calculations for Monolayer MoS2, *Nano Letters* **23**, 3971 (2023), 2212.08451.
- [41] G. Cohen, J. B. Haber, J. B. Neaton, D. Y. Qiu, and S. Refaely-Abramson, Phonon-driven femtosecond dynamics of excitons in crystalline pentacene from first principles, (2023), arXiv:2305.04223.
- [42] J. Pollmann and H. Büttner, Effective Hamiltonians and bindings energies of Wannier excitons in polar semiconductors, *Physical Review B* **16**, 4480 (1977).
- [43] C. D. Spataru and F. Léonard, Tunable band gaps and excitons in doped semiconducting carbon nanotubes made possible by acoustic plasmons, *Physical Review Letters* **104**, 1 (2010), arXiv:1005.0145.
- [44] X. Zhang, J. A. Leveillee, and A. Schleife, Effect of dynamical screening in the Bethe-Salpeter frame-

- work: Excitons in crystalline naphthalene, [, 1 \(2023\)](#), [arXiv:2302.07948](#).
- [45] A. Champagne, J. B. Haber, S. Pokawanvit, D. Y. Qiu, S. Biswas, H. A. Atwater, F. H. da Jornada, and J. B. Neaton, Quasiparticle and optical properties of carrier-doped monolayer MoTe₂ from first principles., Submitted (Nano Letters) [10.1021/acs.nanolett.3c00386 \(2023\)](#).
 - [46] G. D. Mahan, *Many-Particle Physics*, Physics of Solids and Liquids (Springer, 2013).
 - [47] S. Baroni, S. De Gironcoli, and A. Dal Corso, Phonons and related crystal properties from density-functional perturbation theory, [Reviews of Modern Physics **73**, 515 \(2001\)](#), [9702376 \[hep-ph\]](#).
 - [48] Z. Li, G. Antonius, M. Wu, F. H. Da Jornada, and S. G. Louie, Electron-Phonon Coupling from Ab Initio Linear-Response Theory within the GW Method: Correlation-Enhanced Interactions and Superconductivity in Ba_{1-x}K_xBiO₃, [Physical Review Letters **122**, 186402 \(2019\)](#), [arXiv:1902.06212](#).
 - [49] N. E. Lee, J. J. Zhou, H. Y. Chen, and M. Bernardi, Ab initio electron-two-phonon scattering in GaAs from next-to-leading order perturbation theory, *Nature Communications* **11**, [10.1038/s41467-020-15339-0 \(2020\)](#).
 - [50] F. Giustino, M. L. Cohen, and S. G. Louie, Electron-phonon interaction using Wannier functions, [Physical Review B - Condensed Matter and Materials Physics **76**, 1 \(2007\)](#).
 - [51] X.-W. Zhang, K. Xie, E.-G. Wang, T. Cao, and X.-Z. Li, Phonon-mediated exciton relaxation in two-dimensional semiconductors: selection rules and relaxation pathways, [, 1 \(2021\)](#), [arXiv:2110.08873](#).
 - [52] X. W. Zhang and T. Cao, Ab initio calculations of spin-nonconserving exciton-phonon scattering in monolayer transition metal dichalcogenides, *Journal of Physics Condensed Matter* **34**, [10.1088/1361-648X/ac6649 \(2022\)](#), [2202.02866](#).
 - [53] Z. Li, A. M. Alvertis, S. E. Gant, J. B. Neaton, and S. G. Louie, In preparation.
 - [54] J. Deslippe, G. Samsonidze, D. A. Strubbe, M. Jain, M. L. Cohen, and S. G. Louie, BerkeleyGW: A massively parallel computer package for the calculation of the quasiparticle and optical properties of materials and nanostructures, [Computer Physics Communications **183**, 1269 \(2012\)](#), [1111.4429](#).
 - [55] S. Ponce, E. R. Margine, C. Verdi, and F. Giustino, EPW: Electron-phonon coupling, transport and superconducting properties using maximally localized Wannier functions, [Computer Physics Communications **209**, 116 \(2016\)](#), [1604.03525](#).
 - [56] A. Marini, Ab initio finite-temperature excitons, [Physical Review Letters **101**, 1 \(2008\)](#), [0712.3365](#).
 - [57] R. I. Biega, M. R. Filip, L. Leppert, and J. B. Neaton, Chemically Localized Resonant Excitons in Silver-Phosphorus Halide Double Perovskites, [Journal of Physical Chemistry Letters **12**, 2057 \(2021\)](#), [2102.05699](#).
 - [58] M. E. Peskin and D. V. Schroeder, *An Introduction to Quantum Field Theory* (Taylor & Francis group, 1995).
 - [59] K. T. Hecht, *Quantum Mechanics*, Graduate Texts in Contemporary Physics (Springer, 2012).
 - [60] R. Perea-Causin, S. Brem, and E. Malic, Phonon-assisted exciton dissociation in transition metal dichalcogenides, [Nanoscale **13**, 1884 \(2021\)](#), [2009.11031](#).
 - [61] B. A. Lippmann, Rearrangement Collisions, *Physical Review* **102**, 264 (1956).
 - [62] S. Sunakawa, On the Theory of Rearrangement Collisions, *Progress of Theoretical Physics* **24**, 963 (1960).
 - [63] T. B. Day, L. Rodberg, G. Snow, and J. Sucher, Note on Rearrangement Collisions, *Physical Review* **123**, 1051 (1961).
 - [64] C. Coveney, J. Haber, A. M. Alvertis, J. B. Neaton, and M. R. Filip, In preparation.
 - [65] H. Fröhlich, Electrons in lattice fields, [Advances in Physics **3**, 325 \(1954\)](#).
 - [66] G. H. Wannier, The structure of electronic excitation levels in insulating crystals, [Physical Review **52**, 191 \(1937\)](#).
 - [67] N. F. Mott, Conduction in polar crystals. II. The conduction band and ultra-violet absorption of alkali-halide crystals, [Trans. Faraday Soc. **34**, 500 \(1938\)](#).
 - [68] A. Jain, S. P. Ong, G. Hautier, W. Chen, W. D. Richards, S. Dacek, S. Cholia, D. Gunter, D. Skinner, G. Ceder, and K. A. Persson, Commentary: The materials project: A materials genome approach to accelerating materials innovation, *APL Materials* **1**, [10.1063/1.4812323 \(2013\)](#).
 - [69] Y. Zhang, J. Sun, J. P. Perdew, and X. Wu, Comparative first-principles studies of prototypical ferroelectric materials by LDA, GGA, and SCAN meta-GGA, [Physical Review B **96**, 1 \(2017\)](#).
 - [70] P. Giannozzi, S. Baroni, N. Bonini, M. Calandra, R. Car, C. Cavazzoni, D. Ceresoli, G. L. Chiarotti, M. Cococcioni, I. Dabo, A. Dal Corso, S. Fabris, G. Fratesi, S. de Gironcoli, R. Gebauer, U. Gerstmann, C. Gougoussis, A. Kokalj, M. Lazzeri, L. Martin-Samos, N. Marzari, F. Mauri, R. Mazzarello, S. Paolini, A. Pasquarello, L. Paulatto, C. Sbraccia, S. Scandolo, G. Sclauzero, A. P. Seitsonen, A. Smogunov, P. Umari, and R. M. Wentzcovitch, QUANTUM ESPRESSO: a modular and open-source software project for quantum simulations of materials, *Journal of Physics: Condensed Matter* **21**, 395502 (2009).
 - [71] J. P. Perdew, K. Burke, and M. Ernzerhof, Generalized Gradient Approximation Made Simple, *Physical Review Letters* **77**, 3865 (1996).
 - [72] R. O. Jones and O. Gunnarsson, The density functional formalism, its applications and prospects, [Reviews of Modern Physics **61**, 689 \(1989\)](#).
 - [73] S. E. Reyes-Lillo, T. Rangel, F. Bruneval, and J. B. Neaton, Effects of quantum confinement on excited state properties of SrTiO₃ from ab initio many-body perturbation theory, [Physical Review B **94**, 1 \(2016\)](#), [1605.01818](#).
 - [74] A. M. Alvertis, M. D. Ben, H. Felipe, D. Y. Qiu, M. R. Filip, and J. B. Neaton, Importance of nonuniform Brillouin zone sampling for ab initio Bethe-Salpeter equation calculations of exciton binding energies in crystalline solids, [Physical Review B **108**, 1 \(2023\)](#).
 - [75] G. Pizzi, V. Vitale, R. Arita, S. Blügel, F. Freimuth, G. Géranton, M. Gibertini, D. Gresch, C. Johnson, T. Koretsune, J. Ibanez-Azpiroz, H. Lee, J. M. Lihm, D. Marchand, A. Marrazzo, Y. Mokrousov, J. I. Mustafa, Y. Nohara, Y. Nomura, L. Paulatto, S. Poncé, T. Ponweiser, J. Qiao, F. Thöle, S. S. Tsirkin, M. Wierzbowska, N. Marzari, D. Vanderbilt, I. Souza, A. A. Mostofi, and J. R. Yates, Wannier90 as a community code: New features and applications, *Journal of Physics Condensed Matter* **32**, [10.1088/1361-](#)

- 648X/ab51ff (2020).
- [76] J. Voigt, F. Spiegelberg, and M. Senoner, Band parameters of CdS and CdSe single crystals determined from optical exciton spectra, *Physica Status Solidi (B)* **91**, 189 (1979).
 - [77] M. A. Jakobson, V. D. Kagan, R. P. Seisyan, and E. V. Goncharova, Optical properties of "pure" CdS and metal-insulator-semiconductor structures on CdS at electrical operation, *Journal of Crystal Growth* **138**, 225 (1994).
 - [78] T. S. Jeong, P. Y. Yu, and T. S. Kim, Temperature dependence of the free excitons in a CdS single crystal, *Journal of the Korean Physical Society* **36**, 102 (2000).
 - [79] K. Hummer, J. Harl, and G. Kresse, Heyd-Scuseria-Ernzerhof hybrid functional for calculating the lattice dynamics of semiconductors, *Physical Review B - Condensed Matter and Materials Physics* **80**, 10.1103/PhysRevB.80.115205 (2009).
 - [80] M. Lazzeri, M. Calandra, and F. Mauri, Anharmonic phonon frequency shift in MgB₂, *Physical Review B - Condensed Matter and Materials Physics* **68**, 2 (2003), 0306650 [cond-mat].
 - [81] K. Reimann, M. Steube, D. Fröhlich, and S. J. Clarke, Exciton binding energies and band gaps in GaN bulk crystals, *Journal of Crystal Growth* **189-190**, 652 (1998).
 - [82] J. F. Muth, J. H. Lee, I. K. Shmagin, R. M. Kolbas, H. C. Casey, B. P. Keller, U. K. Mishra, and S. P. DenBaars, Absorption coefficient, energy gap, exciton binding energy, and recombination lifetime of GaN obtained from transmission measurements, *Applied Physics Letters* **71**, 2572 (1997).
 - [83] Z. P. Yin, A. Kutepov, and G. Kotliar, Correlation-enhanced electron-phonon coupling: Applications of GW and screened hybrid functional to bismuthates, chloronitrides, and other high-T_c superconductors, *Physical Review X* **3**, 1 (2013), 1110.5751.
 - [84] B. Monserrat, Correlation effects on electron-phonon coupling in semiconductors: Many-body theory along thermal lines, *Phys. Rev. B* **93**, 10.1103/PhysRevB.93.100301 (2016), 0703642 [astro-ph].
 - [85] J. Allerbeck, T. Deckert, L. Spitzner, and D. Brida, Probing free-carrier and exciton dynamics in a bulk semiconductor with two-dimensional electronic spectroscopy, *Physical Review B* **104**, L201202 (2021).
 - [86] A. Jha, H. G. Duan, V. Tiwari, P. K. Nayak, H. J. Snaith, M. Thorwart, and R. J. Dwayne Miller, Direct Observation of Ultrafast Exciton Dissociation in Lead Iodide Perovskite by 2D Electronic Spectroscopy, *ACS Photonics* **5**, 852 (2018).
 - [87] E. H. Bogardus and H. B. Bebb, Bound-exciton, free-exciton, band-acceptor, donor-acceptor, and auger recombination in GaAs, *Physical Review* **176**, 993 (1968).
 - [88] A. K. Viswanath and J. I. Lee, Exciton-phonon interactions, exciton binding energy, and their importance in the realization of room-temperature semiconductor lasers based on GaN, *Physical Review B - Condensed Matter and Materials Physics* **58**, 16333 (1998).
 - [89] J. J. Zhou, O. Hellman, and M. Bernardi, Electron-Phonon Scattering in the Presence of Soft Modes and Electron Mobility in SrTiO₃ Perovskite from First Principles, *Physical Review Letters* **121**, 226603 (2018), 1806.05775.
 - [90] C. Verdi and F. Giustino, Fröhlich electron-phonon vertex from first principles, *Physical Review Letters* **115**, 1 (2015), 1510.06373.
 - [91] C. M. Lueng, H. L. Chan, W. K. Fong, C. Surya, and C. L. Choy, Piezoelectric coefficients of aluminum nitride and gallium nitride, *Journal of Applied Physics* **88**, 5360 (2000).
 - [92] X. Wang, X. He, H. Zhu, L. Sun, W. Fu, X. Wang, L. C. Hoong, H. Wang, Q. Zeng, W. Zhao, J. Wei, Z. Jin, Z. Shen, J. Liu, T. Zhang, and Z. Liu, Subatomic deformation driven by vertical piezoelectricity from CdS ultrathin films, *Science Advances* **2**, 1 (2016).
 - [93] V. A. Jhalani, J. J. Zhou, J. Park, C. E. Dreyer, and M. Bernardi, Piezoelectric Electron-Phonon Interaction from Ab Initio Dynamical Quadrupoles: Impact on Charge Transport in Wurtzite GaN, *Physical Review Letters* **125**, 136602 (2020), 2002.08351.
 - [94] L. Viña, S. Logothetidis, and M. Cardona, Temperature dependence of the dielectric function of germanium, *Phys. Rev. B* **30**, 1979 (1984).
 - [95] S. Logothetidis, L. Via, and M. Cardona, Temperature dependence of the dielectric function and the interband critical points of insb, *Phys. Rev. B* **31**, 947 (1985).
 - [96] L. Via, H. Höchst, and M. Cardona, Dielectric function of α -sn and its temperature dependence, *Phys. Rev. B* **31**, 958 (1985).
 - [97] A. Miyata, A. Mitioglu, P. Plochocka, O. Portugall, J. T. W. Wang, S. D. Stranks, H. J. Snaith, and R. J. Nicholas, Direct measurement of the exciton binding energy and effective masses for charge carriers in organic-inorganic tri-halide perovskites, *Nature Physics* **11**, 582 (2015).
 - [98] C. L. Davies, M. R. Filip, J. B. Patel, T. W. Crothers, C. Verdi, A. D. Wright, R. L. Milot, F. Giustino, M. B. Johnston, and L. M. Herz, Bimolecular recombination in methylammonium lead triiodide perovskite is an inverse absorption process, *Nature Communications* **9**, 1 (2018).
 - [99] J. B. Haber, D. Y. Qiu, F. H. da Jornada, and J. B. Neaton, Maximally localized exciton Wannier functions for solids, *Physical Review B* **108**, 125118 (2023), 2308.03012.
 - [100] S. Sharifzadeh, P. Darancet, L. Kronik, and J. B. Neaton, Low-Energy Charge-Transfer Excitons in Organic Solids from First-Principles: The Case of Pentacene, *The Journal of Physical Chemistry Letters* **4**, 2197 (2013).
 - [101] J. Lafuente-Bartolome, C. Lian, W. H. Sio, I. G. Gurtubay, A. Eiguren, and F. Giustino, Unified approach to polarons and phonon-induced band structure renormalization, *Physical Review Letters* **129**, 76402 (2022), arXiv:2208.06346.
 - [102] H. Kröncke, S. Figge, B. M. Epelbaum, and D. Hommel, Determination of the temperature dependent thermal expansion coefficients of bulk AlN by HRXRD, *Acta Physica Polonica A* **114**, 1193 (2008).
 - [103] D. Strauch, CdS: thermal expansion, in *New Data and Updates for several III-V (including mixed crystals) and II-VI Compounds*, edited by U. Rössler (Springer Berlin Heidelberg, Berlin, Heidelberg, 2012) pp. 97–98.
 - [104] C. Roder, S. Einfeldt, S. Figge, and D. Hommel, Temperature dependence of the thermal expansion of GaN, *Physical Review B - Condensed Matter and Materials Physics* **72**, 1 (2005).
 - [105] N. C. Corsepius, T. C. DeVore, B. A. Reisner, and

- D. L. Warnaar, Using variable temperature powder X-ray diffraction to determine the thermal expansion coefficient of solid MgO, [Journal of Chemical Education](#) **84**, 818 (2007).
- [106] A. Boudali, M. D. Khodja, B. Amrani, D. Bourbie, K. Amara, and A. Abada, First-principles study of structural, elastic, electronic, and thermal properties of SrTiO₃ perovskite cubic, [Physics Letters, Section A: General, Atomic and Solid State Physics](#) **373**, 879 (2009).
- [107] C. Fennie and K. Rabe, Structural and dielectric properties of Sr₂TiO₄ from first principles, [Physical Review B - Condensed Matter and Materials Physics](#) **68**, 1 (2003), 0305266 [cond-mat].